ABSTRACT

KERRIGAN, SEAN PATRICK. Development, Fabrication, and Characterization of Piezoelectric Non-Intrusive Wireless Vibration Sensors for Nuclear Power Plant Applications. (Under the direction of Dr. Mohamed Bourham and Dr. Xiaoning Jiang).

The Very-High Temperature Reactor (VHTR) is a proposed generation IV reactor design that can reach operating temperatures of 1000 °C. The next generation of nuclear power plants offer a material challenge to current reactor sensing technologies. Development of wireless, non-intrusive aluminum nitride (AlN) based piezoelectric vibration sensors aims to provide the VHTR with reliable and safe sensing in the environment of high-temperatures, irradiation, and corrosion.

A piezoelectric AlN-based accelerometer was designed and fabricated using bulk AlN and Inconel 601 as the housing and seismic mass. The sensor was shown to have a working frequency range up to 600 Hz, which is ideal for structural damage detection within a nuclear power plant. A multi-axial accelerometer was fabricated using three AlN single crystals as the piezoelectric sensing elements in order to determine the location of the vibrational source.

The effect of radiation, high-temperature, and corrosion on the AlN single crystal sensing elements were explored. AlN single crystal samples and a fully fabricated sensor were irradiated using a Co-60 gamma source for periods of 1 and 2 months. The analysis of the sensor performance post-irradiation showed no significant change in the output signal. The surface topography of the samples post-irradiation was observed using SEM and EDS characterization techniques. No changes in the surface were observed. The effect of neutrons on the AlN single crystals was simulated using a heavy-ion beam. The results showed that Inconel 601 provides strong shielding to the AlN single crystals from incoming particles. The angle of the incoming particles affects the penetration depth of the particles.

The sensor and AlN single crystals were exposed to high-temperatures up to 1000 °C using an industrial furnace. The tests showed constant performance up to 1000 °C while a long-exposure test showed visible charring on the sensor housing. The developed accelerometer was able to successfully acquire data at temperatures up to 1000 °C, and the wireless communications system was able to transmit the data reliably and efficiently.

The effects of corrosion on the sensor can impact the performance and expected operational lifetime of the sensor. Cyclic polarization corrosion tests were performed to determine the corrosion rate of the AlN single crystals. Corrosion experiments were run at pH values of 3 and 6 and temperatures up to 200 °C. The effect of thin-film coatings of ZrO_2 on the sensor's corrosion resistance was investigated. AlN samples were irradiated using a Co-60 gamma source for periods of 1 and 2 months to investigate the effect of corrosion on irradiated samples. The addition of thin-film coatings of ZrO_2 showed improved corrosion resistance especially at higher temperatures compared to the bare substrates. The irradiated samples showed similar corrosion behavior, yet the corrosion rate of the irradiated samples was higher than the unirradiated bare samples. The estimated operational lifetimes of the AlN sensing elements showed that AlN piezoelectric accelerometers could be an asset to next generation of nuclear power plants especially if thin-films or other shielding methods are employed to control the radiation and temperature effects of the environment.

The characterization of the AlN sensing elements showed the robustness of the material against high-temperatures, irradiation, and corrosion effects. Piezoelectric AlN-based vibration sensors that were fabricated and tested showed the applicability to be outfitted to the next generation of nuclear power plant designs.

Development, Fabrication, and Characterization of Piezoelectric Non-Intrusive Wireless Vibration Sensors for Nuclear Power Plant Applications

by
Sean Patrick Kerrigan

A dissertation submitted to the Graduate Faculty of
North Carolina State University
in partial fulfillment of the
requirements for the degree of
Doctor of Philosophy

Nuclear Engineering

Raleigh, North Carolina
2023

APPROVED BY:

Dr. Mohamed Bourham Co-chair of Advisory Committee	Dr. Xiaoning Jiang Co-chair of Advisory Committee
Dr. Xu Wu	Dr. John G. Gilligan
Dr. Ralph Smith	

DEDICATION

To my family and to my wife Fatma for their ceaseless support, motivation, and encouragement.

BIOGRAPHY

Sean Patrick Kerrigan was born on May 6, 1993 in Fairfax, Virginia. He attended Gonzaga College High School in Washington, D.C., graduating in 2011. Sean attended Virginia Polytechnic Institute and State University (Virginia Tech), where he earned his Bachelor's degree in Chemical Engineering in 2015. He then attended the University of Florida where he earned his Master's of Material Science & Engineering in 2017. Finally, Sean earned his Master's of Nuclear Engineering at North Carolina State University in 2020 under the direction of Dr. Mohamed Bourham. He has spent the past few years performing materials research to develop instrumentation and controls that can survive the extreme environments of the planned next generation nuclear reactors. Sean would like to continue to pursue his interest in researching new materials for extreme environments, specifically coated materials, new alloys, and corrosion or radiation resistive materials.

ACKNOWLEDGMENTS

I would like to thank my advisors, Dr. Mohamed Bourham and Dr. Xiaoning Jiang. Initially joining the Nuclear Engineering department in 2017, Dr. Bourham was always available to help me acclimate to the university and the department. He would always set aside time to check on how your experiments were progressing and discuss despite his incredibly busy schedule. I am incredibly thankful for the opportunity to work under his direction and for the assistance he has provided me throughout graduate school. I would like to thank Dr. Xiaoning Jiang for the opportunity to join his lab group and learn several topics in Mechanical Engineering that were completely new to me. He always tried to push you to achieve something great and understand what is happening in your data.

I would also like to thank my committee members Dr. John Gilligan, Dr. Xu Wu, and Dr. Ralph Smith for their feedback on my research throughout the graduate school process.

I would like to thank the Department of Energy (DoE) Nuclear Energy University Program (NEUP) for providing financial support for this project under contract DE-NE0008708 Project NEUP 17-12703.

I would like to thank Ervin Miller for his time teaching me and passing on his knowledge from years in industry. I would like to thank Emad Tawadrous from the machine shop for aiding in fabricating tough to machine parts throughout this project.

I would like to thank my collaborators on this project, Dr. Bharat Balagopal from the Electrical Engineering Department and Dr. Howuk Kim from the Mechanical & Aerospace Engineering Department. Additionally, I would like to thank all my colleagues from Dr. Jiang’s lab who helped me throughout the development of fabricating an accelerometer.

I would like to thank my friends that have always been with me throughout graduate school, making memories and connections that I hope will last forever.

Finally, I would like to thank my wife Fatma. None of this would have been possible without her guidance and support. Having met during graduate school, she made the journey enjoyable. I thank her for all the support and encouragement shown throughout graduate school.

TABLE OF CONTENTS

LIST OF TABLES

LIST OF FIGURES

CHAPTER 1

INTRODUCTION

Nuclear power plants (NPP) utilize a combination of over 10,000 sensors and detectors to monitor system performance [1]. These sensors are used for a wide array of processes such as preventative maintenance monitoring, liquid level sensing, temperature control, pressure monitoring, and flow control [2]. Each of these processes are directly monitored and controlled by reactor operators who rely on information output from various types of sensors. Sensors measure different physical parameters and convert them into an electrical signal that can be manipulated using electronics [3]. Sensors operating reliably and safely ensure that nuclear power plants generate continuous energy to the electrical grid without interruptions. In the case of an unexpected system change, the sensors provide real-time performance changes to power plant operators who can control the status of the reactor. Sensors and detectors are the primary tool for understanding the changes occurring within a reactor.

The next generation of reactors (Gen. IV) consists of reactor designs that operate at much higher temperatures compared to currently operating commercial reactors. The Very-High-Temperature Reactor (VHTR) is an example of one of the Generation IV designs that can reach operating temperatures of 1000 °C [4]. The VHTR is an attractive design as the high-temperature operating cycle provides higher thermal efficiency over the current low-temperature fleet of reactors [5]. Traditionally, sensors are placed invasively within the reactor and thus will not be able to survive the harsh operating environment of the VHTR. Non-invasive sensors are being designed to reliably function at elevated temperatures to be fitted to the next generation of reactors.

1.1 Nuclear Power Plant Instrumentation

Nuclear power plants use instrumentation and controls (I&C) to operate efficiently and safely. I&Cs provide the NPP operators with detailed information about the current operating status of the NPP, thus allowing the operators to make informed decisions when controlling the system [6]. I&Cs allow for automatic control of the NPP system, thus the reactor operator does not need to manually change certain system parameters as the I&Cs will measure a shift in one system parameters and automatically adjust other parameters to ensure the NPP continues to operate safely at the desired power level. I&Cs act as a safety measure by constantly measuring the changes made through operator manual controls or automatic controls. The instrumentation has set threshold limits, which trigger internal alarms if the operator or automatic controls make a mistake. Throughout the development of nuclear power, NPPs have utilized a variety of different types of I&Cs to ensure safe and efficient operation. NPPs use a three-level structure (the Equipment, System, and Plant levels) for digital I&C operation as shown in Fig. 1.1. Sensors are placed either within or onto the equipment to be measured, thus sensors fall within the equipment level of the control system. The sensor output is connected to remote monitoring units at the system level, and the output of the monitoring units is digitally displayed at the plant level for reactor operators on either the plant computer system or a system alarm.

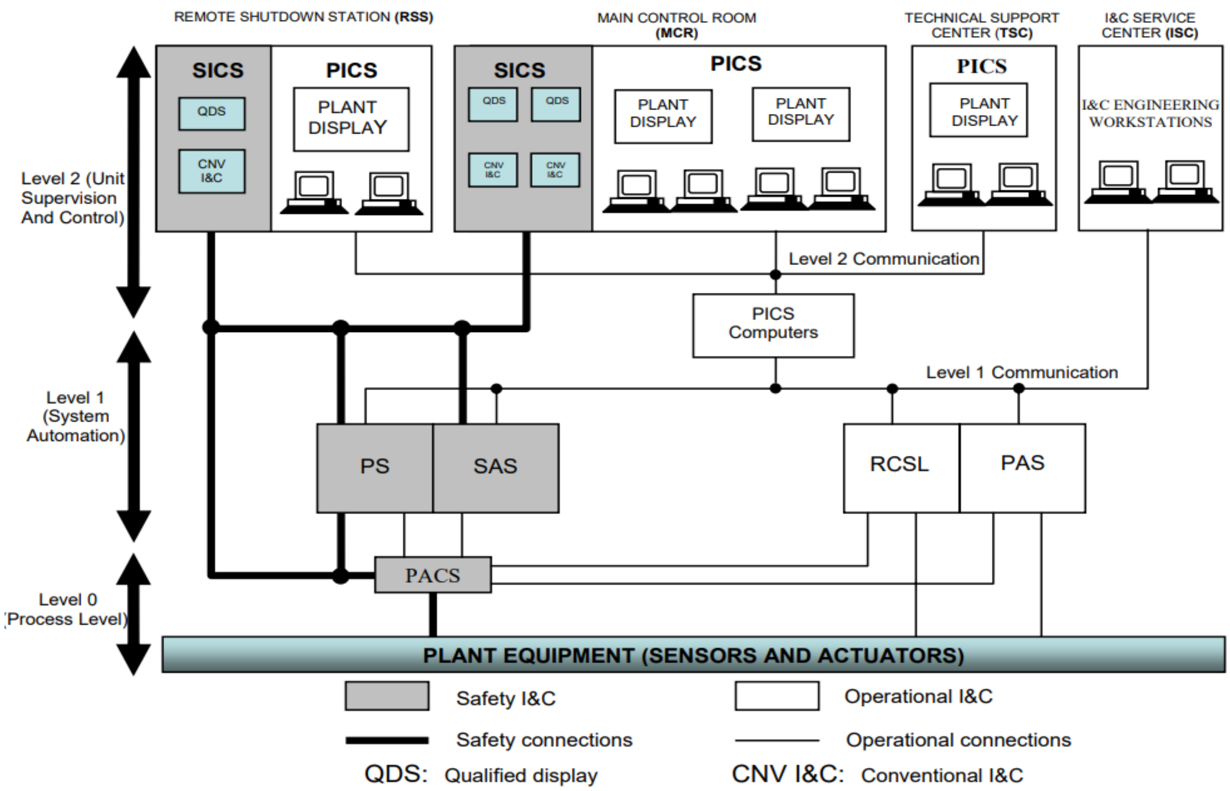

Figure 1.1. Integrated digital control system and levels within NPPs [1].

Within NPPs, there are a variety of different sensors to monitor the system's pressures, temperatures, flow rates, liquid levels, vibrations, and radiation levels. The sensor locations vary by power plant design, but the sensor locations for a Pressurized Water Reactor (PWR) are shown in Fig. 1.2. The two-loop reactor design uses flow and temperature sensors to monitor the status of the hot leg and cold leg streams that enter and exit the reactor core. Liquid level measurements are typically taken within any tank such as the core, pressurizer, and steam generator.

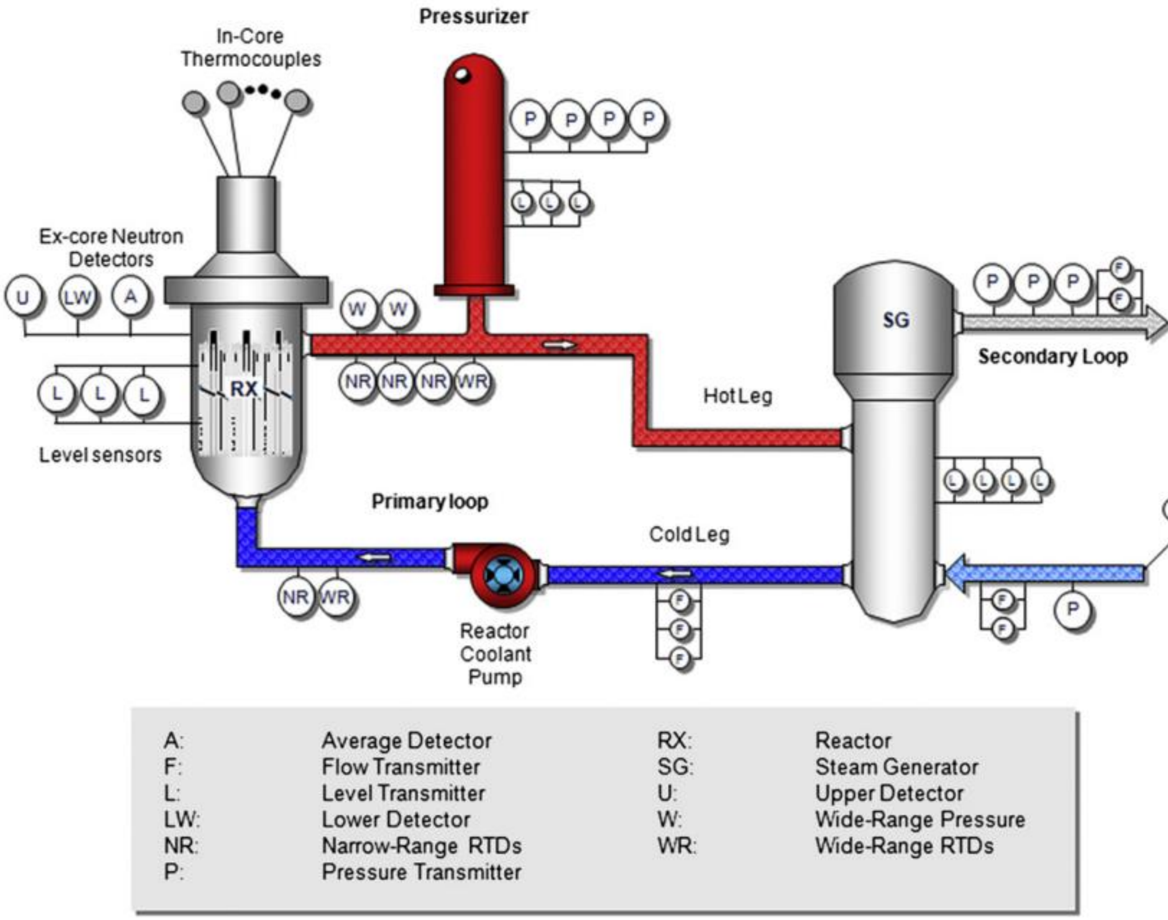

Figure 1.2. Sensor locations in a Pressurized Water Reactor [7].

1.1.1 Types of Sensors

The instrumentation and controls used within currently operating nuclear power plants have not changed significantly from conventional instrumentation [8]. A few examples of currently used sensors include liquid level sensors, pressure monitoring sensors, temperature sensors, flow rate sensors, stress sensors, radiation detectors, and vibration sensors. Different types of sensors use a wide variety of different sensing technologies to measure physical phenomenon. As mentioned previously, then next generation of reactors calls for improved sensors to withstand the high-temperature environment of the VHTR. Instrumentation technologies are being outfitted specifically to fit new NPP environmental conditions rather than inventing entirely new types of sensors [8]. By adapting previously used sensing technologies to withstand harsh environments, the developed sensors are applicable to almost every NPP design.

Temperature measurements are taken across the NPP as the temperature of hot leg and cold leg flow streams can determine the economic efficiency of producing steam. Thermocouples are the most common sensor for measuring temperature. A thermocouple is formed by building a circuit using two different metals [3]. The metals are connected at the measurement junction, as shown in Fig. 1.3. The measurement junction is inserted into the process of interest, and the output is relayed to a digital display. Thermocouples have no active sensing element, thus they are able to be used at very high temperatures because the thermocouple is not limited by typical sensing element material properties. There are several different types of thermocouples, which depend on the two different materials being used. The chosen materials also determine the operating temperature range of the thermocouple.

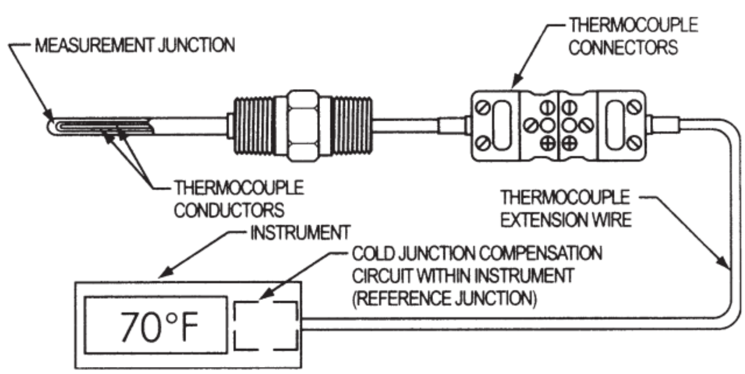

Figure 1.3. Thermocouple design using two different conductive materials [3].

Resistive Temperature Devices (RTDs) offer temperature measurements by exposing an active sensing element to the process temperature. The sensing element changes its resistance when it experiences a temperature change, thus this change can be used to determine the temperature of the process being measured [3]. An example of a fabricated RTD is shown in Fig. 1.4. RTDs are limited by the material constraints of the active sensing element, thus RTD development must be specifically designed for applications involving harsh environments.

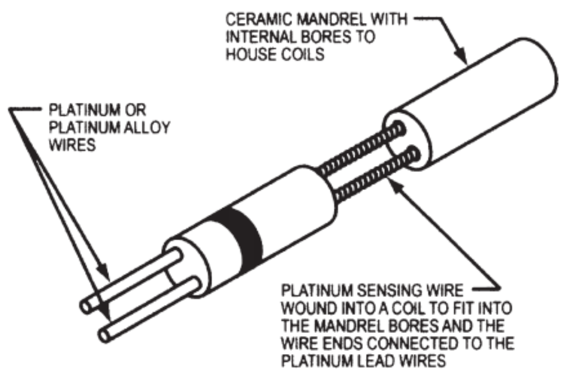

Figure 1.4. Basic structure of a coil-type RTD for temperature measurements [3].

Liquid level sensors have a dual purpose within NPPs. The first purpose is to ensure tanks holding liquid do not either overflow or dry out as both of these scenarios can result in catastrophic consequences. Additionally, the liquid level is measured to verify readings from in-line flow sensors to ensure the difference between the inlet and outlet flow are match, resulting in a constant liquid level [3]. Liquid level sensors use a variety of different sensing technologies, such as liquid level floats, differential pressure transmitters, and ultrasonic liquid level sensors. Liquid level floats use a buoy to measure the liquid level using the wall of the tank as a measurement tool. Ultrasonic level sensors utilize sound waves to measure a reflected signal off the surface of the liquid. The time between the transmitted and received reflected signal indicates the distance between the sensor and the liquid level, thus the liquid level can be determined.

Nuclear power plants utilize flow rate sensors to ensure the inlet and outlets of various cooling lines provide enough coolant to the reactor core [3]. Differential pressure sensors are the most commonly used type of liquid flow sensor. These type of sensors operate by utilizing the Venturi effect in which a pressure loss across the pipe is induced by forming a restriction in the flow path as shown in Fig. 1.5 [3]. The flow rate (Q) can be calculated using the following equation derived from the Bernoulli equation:

$$Q = vA = k_{dis\ coeff} \left(\frac{\Delta P}{\rho}\right)^{\frac{1}{2}} A \tag{1.1}$$

In which v is the velocity of the liquid, A is the cross sectional area of the pipe, $k_{dis\ coeff}$ is the discharge coefficient, ΔP is the pressure drop across the pipe, and ρ is the mass density of the liquid.

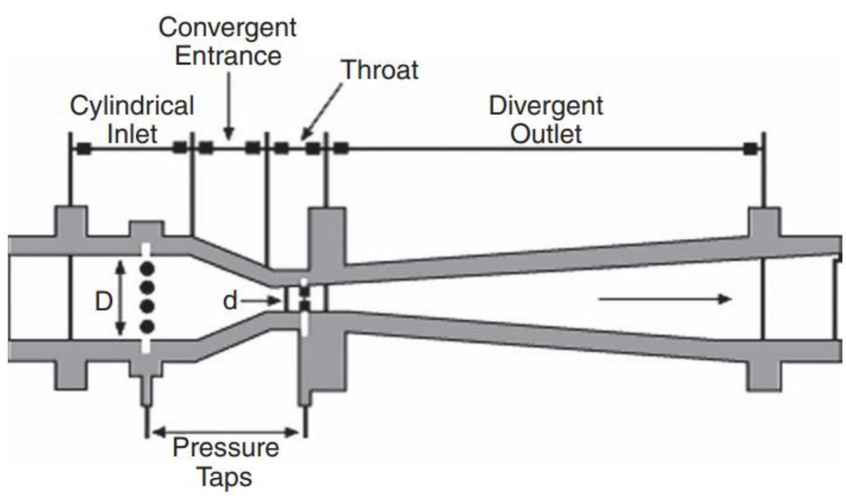

Figure 1.5. Illustration of the Venturi effect across a pipe to determine the liquid flow rate [3].

Vibration sensors, also referred to as accelerometers, monitor the integrity of structural components within nuclear power plants to ensure they operate safely and reliably. By implementing vibration sensing technologies within a nuclear power plant, preventative maintenance can be employed to monitor the structural integrity of key NPP components [2]. Preventative maintenance allows for less plant downtime due to maintenance and thus more reliable operation. Vibration sensors performance depend on the choice on sensing technology used and the sensing element selected. These decisions heavily impact the performance of vibration sensors across a wide range of environmental conditions. An example of a piezoelectric vibration sensor is shown in Fig. 1.6. The sensor is mounted to a base, which would be the structure being measured. The piezoelectric sensing element experiences shear or compression deformation as a result of an applied acceleration or vibration leading to the buildup of an electrical charge by the piezoelectric material [3].

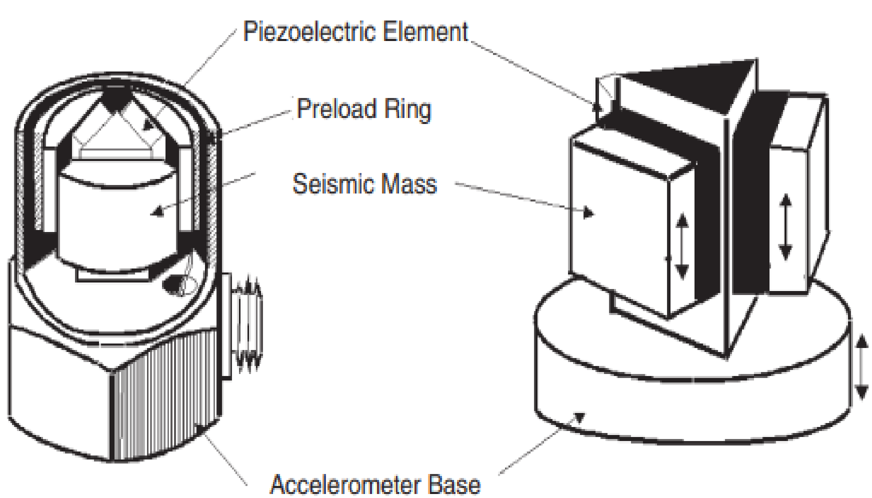

Figure 1.6. Basic piezoelectric vibration sensor design [3].

1.2 Motivation and Goal of Research

As Chapter 1 demonstrated the vast array of sensors utilized throughout the nuclear power plant, these sensors will not survive within the operating environment of the VHTR. As such, there is a need to develop new sensors that can be outfitted to the next generation of nuclear power plant designs. The criteria for these fabricated sensors are to operate under high-temperature, exhibit radiation resistant properties, and corrosion resistant properties. The techniques currently utilized by operating commercial nuclear power plants mainly involve intrusive sensing, meaning the sensor is placed within the reactor. This causes the sensor to be exposed to the environmental conditions of the reactor and enables the sensor to be a potential safety risk to the reactor. The next generation of nuclear power plants needs to develop wireless sensing techniques to allow for non-intrusive sensing to occur. This project aims to create a sensor to address these concerns.

This research focuses on the development, fabrication, and testing of aluminum nitride (AlN) based non-intrusive wireless piezoelectric vibration sensors for use in nuclear power plants. The focus on this project involves developing vibration sensors using bulk piezoelectric sensing elements as reliable vibration sensors can predict maintenance schedules for key reactor components, thus limiting the plant's downtime due to unexpected maintenance. By developing non-intrusive wireless sensors for NPPs, the sensors are placed in areas with less severe environmental conditions, thus extending sensor lifetime and allowing the sensors to be accessed routinely. This dissertation covers the fabrication and development of a bulk AlN-based piezoelectric vibration sensor, the characterization of the sensor under the effects of the VHTR environmental conditions (radiation, high-temperature, and corrosion), and the testing of the wireless communication transfer of the sensor data under while the sensor is exposed to high-temperatures.

Currently operating nuclear power plants utilize invasive sensors, meaning the sensor is located inside the containment structure of the NPP. This presents challenges during maintenance as the sensor may not easily be accessed depending on the contact location. Non-intrusive sensors operate by transmitting data wirelessly to a digital display system. This is a significant advantage over current sensing techniques as it provides non-intrusive sensing technology to NPP instrumentation. Utilizing the benefits of wireless communication, nuclear power plant sensors can be replaced easier, meaning less plant maintenance downtime [11]. This will in turn lead to more long term profits for commercial nuclear use as the plant will not need to be shut down for maintenance issues. The sensor communication setup captures real time system measurements, thus plant operators can ensure the reactor operates safely to generate reliable energy to the grid. By developing sensing methods that operate non-intrusively, the sensor can be located outside of harsh environments while still measuring the process reliably.

1.3 Dissertation Outline

The outline of this dissertation is as follows: Chapter 1 provides an introduction into nuclear power plant instrumentation. It covers various types of sensors used throughout a nuclear power plant and a few of the sensing technologies utilized within these sensors. Chapter 2 discusses the piezoelectric effect, which is the concept the fabricated vibration sensor is based on. The design and fabrication of the piezoelectric vibration sensor are discussed as well as an overview of various piezoelectric materials. The design of a multi-axial vibration sensor is also discussed and simulated. Chapter 3 discusses the development of a mock-up experiment to test the vibration sensor in real time. Results from the preliminary sensor measurements are discussed. Chapter 4 discusses the characterization of the sensor's active sensing element, AlN, and the entire constructed sensors response to irradiation. Chapter 5 discusses the performance of the vibration sensor while exposed to high-temperatures. Chapter 6 discusses the corrosion analysis of the AlN sensing element used within a fabricated vibration sensor. Chapter 7 provides a summary of the project, conclusions reached from the design and characterization work of the vibration sensor, and future work that could be performed to expand the project's scope. Finally, this is followed by the Appendix.

1.4 References

[1] Korsah, K. (2009). *Instrumentation and controls in nuclear power plants: An emerging technologies update*. U.S. Nuclear Regulatory Commission, Office of Nuclear Regulatory Research.

[2] Kothamasu, R.; Huang, S. H.; VerDuin, W. H. System Health Monitoring and Prognostics—a Review of Current Paradigms and Practices. The International Journal of Advanced Manufacturing Technology, 2006, 28, 1012-1024

[3] Wilson, J. S. (2005). Sensor Technology Handbook. Newnes.

[4] Ingersoll, D. T.; Status of Physics and Safety Analyses for the Liquid-Salt-Cooled Very High-Temperature Reactor (LS-VHTR). ORNL/TM-2005/218, US Department of Energy, 2005.

[5] Breeze, P. (2019). Nuclear power. Power Generation Technologies, 399–429. https://doi.org/10.1016/b978-0-08-102631-1.00017-1

[6] IAEA. (1984). Nuclear power plant instrumentation and control: A guidebook.

[7] H. M. Hashemian, “On-line monitoring applications in nuclear power plants,” Progress in Nuclear Energy, Vol. 53, No. 2, pp. 167-181, 2011.

[8] Sabharwall, P., O’Brien, J. E., Yoon, S. J., Sun, X. (2015). Experimental Facility for development of high-temperature reactor technology: Instrumentation needs and challenges. EPJ Nuclear Sciences Technologies, 1, 14. https://doi.org/10.1051/epjn/e2015-50011-8

[9] Kitada, Y.; Hirotani, T. Iguchi, M. Models Test on Dynamic Structure–Structure Interaction of Nuclear Power Plant Buildings. Nuclear Engineering and Design, 1999, 192, 205-216

CHAPTER 2

PIEZOELECTRIC VIBRATION SENSORS

2.1 Background

2.1.1 Piezoelectrics

The piezoelectric effect, discovered by Jacques and Pierre Currie in 1880, is the generation of an electrical charge within a material in the presence of an applied mechanical stress [1]. The Currie brothers showed the piezoelectric effect using Quartz crystals under applied pressure. A shear type accelerometer operates as the relative motion between the base structure and the seismic mass causes a shear of the active sensing element. This shear deformation generates an electrical charge due to the piezoelectric effect. The general equation for this vibration sensing phenomenon is shown below:

$$m\ddot{y} + c\dot{y} + ky = m\ddot{x}_b \tag{2.1}$$

Where:

m is the seismic mass,

c is the damping coefficient,

k is the spring constant,

y is the relative motion between the base and the seismic mass

Piezoelectric sensors operate by generating an electrical charge in the presence of an applied stress. The operational mode of the piezoelectric sensor depends on the type of sensor and the selected piezoelectric material being used. The performance of the piezoelectric material depends on the environmental conditions of the sensor. Piezoelectric sensors have a simple structure, are cost effective, and high frequency resolution making them favorable for NPP applications if they can survive the harsh environment [2].

2.1.2 Types of Piezoelectric Materials

The piezoelectric effect depends upon the material being used, thus there are certain types of piezoelectric materials that need to be considered given the application of your project. Material selection is an important process when trying to fabricate materials for specific applications. Piezoelectrics fall into four main classes of materials: ceramics, organic and inorganic composites, polymers, and single crystals [3]. Material properties of common piezoelectric materials are shown in Table 2.1 below.

Table 2.1. Material properties of piezoelectric materials [4-10].

Material Property	**Symbol**	**Units**	**Materials**					
			BaTiO3	**PZT-4**	**PVDF**	**SiO2**	**LiNbO3**	**AlN**
Curie temperature	T_c	°C	120	328	-	-	1140	1200
Density	ρ	g/cm3	6.02	7.7	1.8	2.2	4.7	3.3
Coupling coefficient	k_t	-	0.38	0.51	0.3	0.09	0.49	0.24
Piezoelectric constant	d_{33}	pC/N	190	289	33	2.3	4.9	5.5
Dielectric permittivity	ε_{33}	-	1700	700	10	4.68	39	10.7
Stiffness	c_{33}	GPa	108	150	8.5	105.8	250	420

Piezoelectric ceramics are man-made piezoelectric material through the polarization process. The poling process occurs by exposing the material to a high intensity electric field. The applied electric field causes the dipoles in the structure to align, thus making the material piezoelectric. Piezoelectric ceramics are the most commonly used piezoelectric materials. Barium titanate ($BaTiO_3$) is a commonly used piezoceramic material that maintains a perovskite structure and high piezoelectric coefficient [11]. In terms of piezoceramics, lead zirconium titanate (PZT) is most used piezoelectric due to its low costs, ease of manufacturing, and improved sensitivity when compared to $BaTiO_3$. Variations of PZT have also been researched by adding small amounts of additives to the mix to form PZT-based ceramics such as $Pb(B_1B_2)O_3$ [12].

Polyvinylidine fluoride (PVDF) is a favorable piezoelectric polymer due to its flexible structure, cost effectiveness, and low acoustic impedance [6]. Polymeric piezoelectric materials are limited in their applications due to low electromechanical coupling and dielectric losses. Polymeric piezoelectrics are being investigated for use in a variety of sensing applications using thin films.

Piezoelectric composites are formed through the combination of a piezoelectric material with a polymer. Composite materials are commonly used in biomedical imaging technology due to the low acoustic impedance matching the impedance of human tissue. The limiting factor for applications involving piezoelectric composites often depends on the survival of the polymer material selected [13]. At elevated temperatures, piezocomposites often exhibit low thermal conductivity and high thermal expansion, making them undesirable for applications such as the VHTR.

The classic example of single crystals being used in piezoelectrics begins with the first discovery by the Currie brothers using quartz (SiO_2). Quartz offers high electrical resistivity and stability at high temperatures until it experiences a phase transition at temperatures higher than 450 °C [7]. Lithium niobate ($LiNbO_3$) is a promising material for room temperature application due to its strong electromechanical coupling, but $LiNbO_3$ experiences decomposition at temperatures as low as 300 °C [14]. The temperature limitations of $LiNbO_3$ crystals exclude it as a candidate for nuclear power plant sensors, especially when looking at the VHTR design specifically. Gallium orthophosphate ($GaPO_4$) has shown to be resistant to temperature up to 1000 °C, making it a desirable material for high-temperature application such as the VHTR [15]. The other material that maintains a high Currie temperature is aluminum nitride (AlN), which exhibits piezoelectric properties until temperatures above 2000 °C [16]. AlN crystals have high thermal conductivity, small thermal expansion, and high electric resistivity making it an ideal material for nuclear power plant applications [8].

Each piezoelectric material offers different advantages in terms of piezoelectric effect strength, durability, resistance to electrical interference, but the major limitation of most materials is the temperature range. The project application sets the criteria for material selection, hence the VHTR demands materials that can withstand operating temperatures upwards of 1000 °C. The operating temperature difference between various piezoelectric materials is shown in Fig 2.1. The piezoelectric single crystals maintain an operational range up to 1000 °C, making them the only class of piezoelectric materials capable for use in VHTR applications.

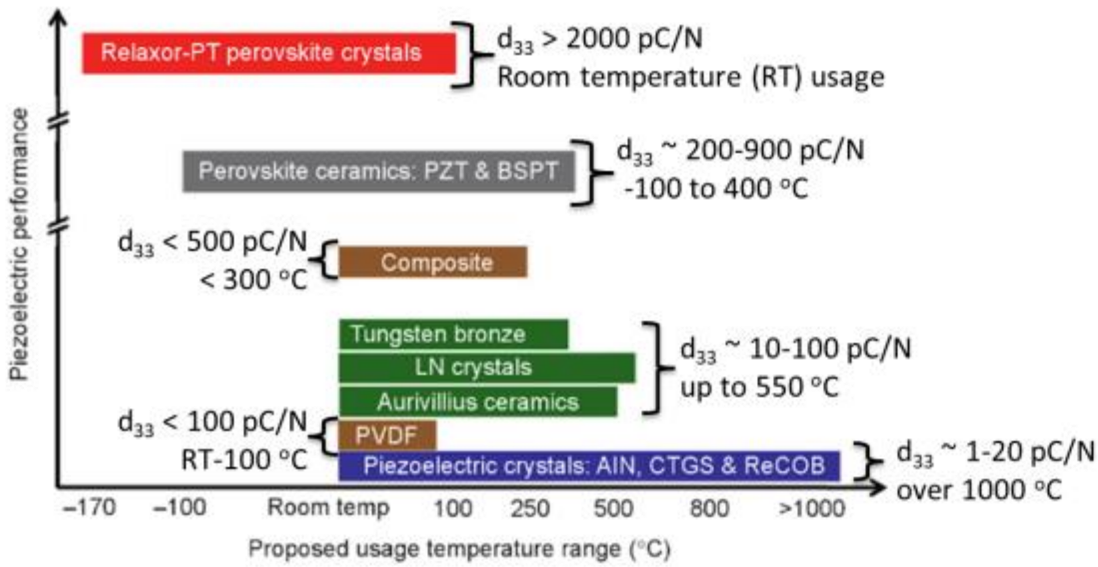

Figure 2.1. Comparison of piezoelectric materials across a wide temperature range [13].

2.1.3 Recent Applications

Piezoelectrics have been used across a variety of different fields, including the medical industry, biomedical industry, nuclear energy industry, and the consumer electronics. Piezoelectrics have been used in vibration sensing for structural monitoring, energy harvesting, ultrasound transducers, and advanced biomedical imaging. Piezoelectric sensors have been designed to measure physical properties such as acceleration, pressure, and rotation and tilt. Fig. 2.2 (a) shows a fabricated wearable biomedical application of piezoelectrics by measuring the arterial pulse using ultrathin PET as the piezoelectric material [17]. Fig. 2.2 (b) shows the fabrication of biodegradable pressure sensor created using a thin film of β-glycine in a chitosan matrix [18]. Fig. 2.2 (c) shows a fabricated high-temperature accelerometer using $YCa_4O(BO_3)_3$, known as YCOB, as the active sensing element [19]. The accelerometer using YCOB as the active sensing element was able to reach temperatures of 1000 °C. Fig. 2.2 (d) shows the application of using piezoelectrics to perform energy harvesting, which is ideal due to the focus on expanding renewable energy techniques [20]. Piezoelectric devices are fabricated using a variety of different sensing materials for use in applications spanning multiple academic disciplines.

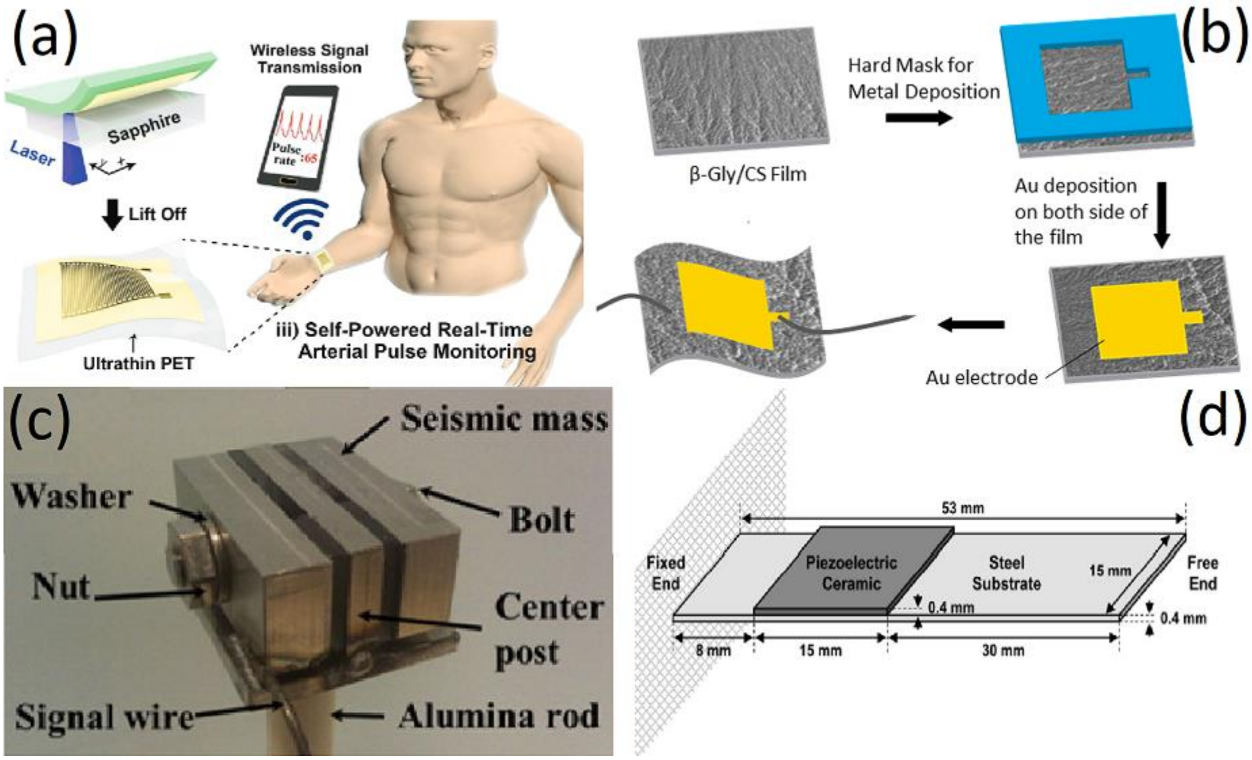

Figure 2.2. Applications using piezoelectric transducers such as (a) pulse monitoring for fitness applications [17], (b) biodegradable pressure sensing [18], (c) high-temperature vibration sensing using YCOB [19], and (d) piezoelectric energy harvesting system [20].

2.2 Objectives

The objective of this research aims to design, fabricate, and test a multi-axial AlN-based vibration sensor for use in the next generation of nuclear power plant designs. The design criteria for these sensors must be able to operate at ~1000 °C. The design will employ a shear-type sensor that utilizes bulk machined AlN material for higher sensitivity. By utilizing several uni-axial vibration sensors at the same time, the difference in output signal from each sensor can be used to determine the location of the incoming vibration signal. This information is useful when trying to identify the source of a vibration signal within a NPP.

2.3 Materials & Methods

2.3.1 Sensor Design and Fabrication

The vibration sensor is fabricated according to the schematic in Fig. 2.3 (a). The uni-axial design's fabrication details were published by Kim et al. [21]. The seismic masses are constructed of Inconel 601 using a mass of 9.4 g. Inconel 601 maintains a low rate of thermal expansion making is a desirable material for use in VHTR applications [9]. The sensors are fabricated using AlN single crystals (7 mm×7 mm×0.8 mm) produced by HexaTech Inc. The side walls of the crystals are deposited with a thin layer of gold electrodes. The AlN single crystal plated with gold electrodes is placed between two seismic masses of known mass. The output of the sensor is relayed using connected platinum wires to each of the AlN sensing elements. The sensing elements are secured to the sensor base using a high-temperature thermal paste for insulation. The entire sensor is secured and mounted using screws and nuts to ensure the sensors holds together during the shear deformation. A fully constructed sensor can be seen in Fig. 2.4.

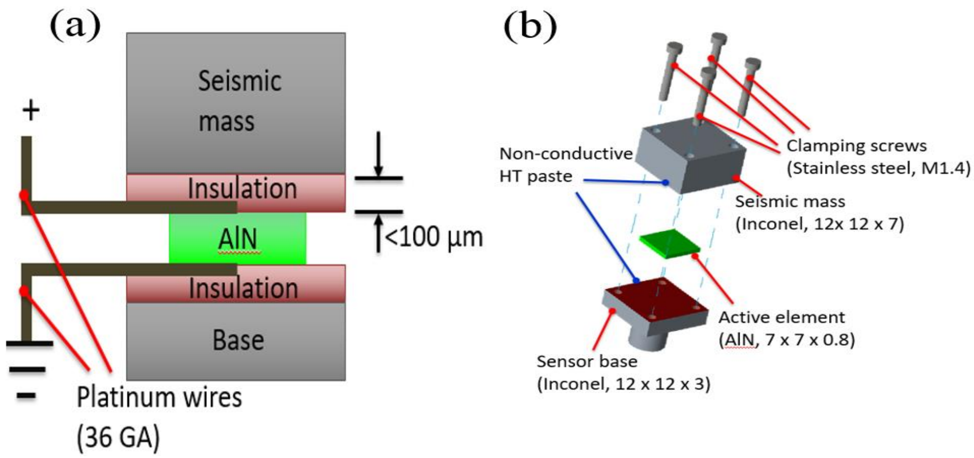

Figure 2.3. Operating principle of the AlN-based piezoelectric vibration sensor (a), and a schematic of a constructed AlN vibration sensor (b).

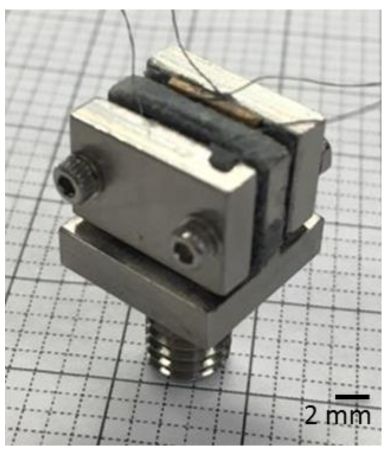

Figure 2.4. Fabricated high-temperature AlN-based accelerometer using Inconel 601 as the seismic masses [21].

The multi-axial sensor is fabricated using the same methods utilized in the uni-axial sensor. The simulation model is constructed using Ansys Software, shown in Fig. 2.5. The multi-axial sensor has three AlN sensing elements all held tight to the seismic mass using Inconel base plates.

The sensor was machined and fabricated using stainless steel screws, Inconel 601 seismic mass and base plates, as shown in Fig. 2.6.

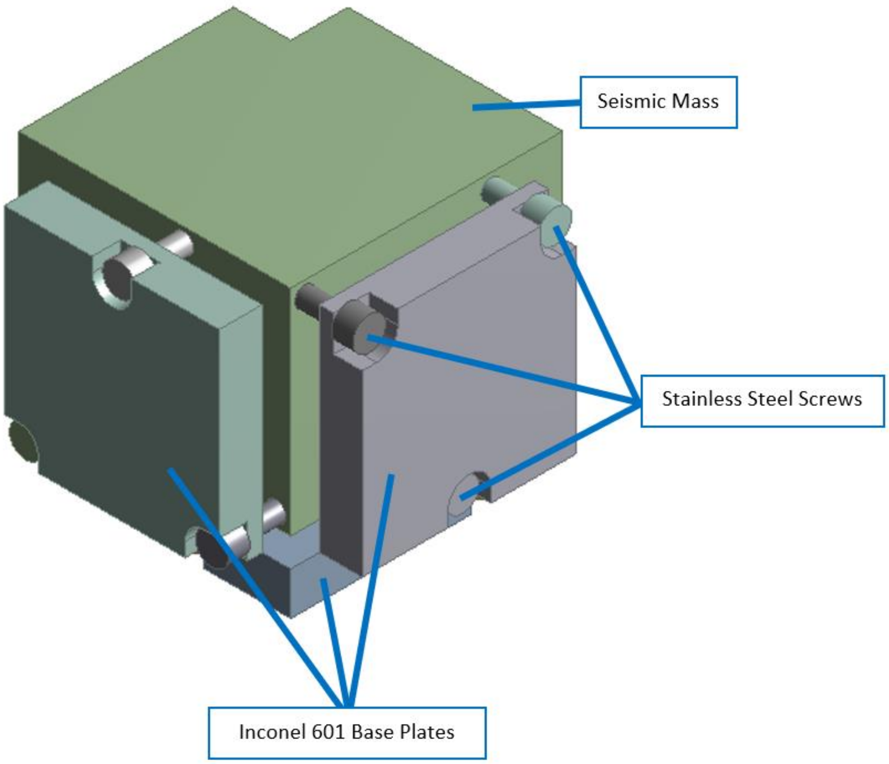

Figure 2.5. Ansys constructed model of multi-axial vibration sensor.

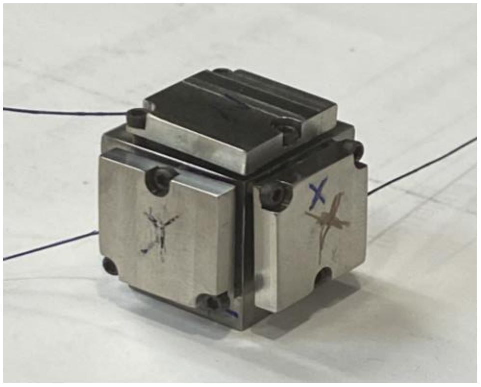

Figure 2.6. Fabricated high-temperature AlN-based multi-axial accelerometer using Inconel 601 as the seismic masses.

2.4 Results and Discussion

2.4.1 Simulation Results

Simulations of the performance of the vibration sensor were run using single sensors and multiple sensors operating simultaneously. Input accelerations were generated from 1g to 3g in various angles to induce multiple sensor responses. The results of an input vibration at a 45° angle to the sensor with an acceleration of 1g in the x-axis and the y-axis is shown in Fig. 2.7 below. The resonance peak shows a distinct difference between the measured values of the different axial sensors. The difference between the output of the sensors in the low frequency region (<1000 Hz) showed a minor difference that needed to be improves as the majority of structural integrity monitoring within nuclear power plants occurs at frequencies below 400 Hz.

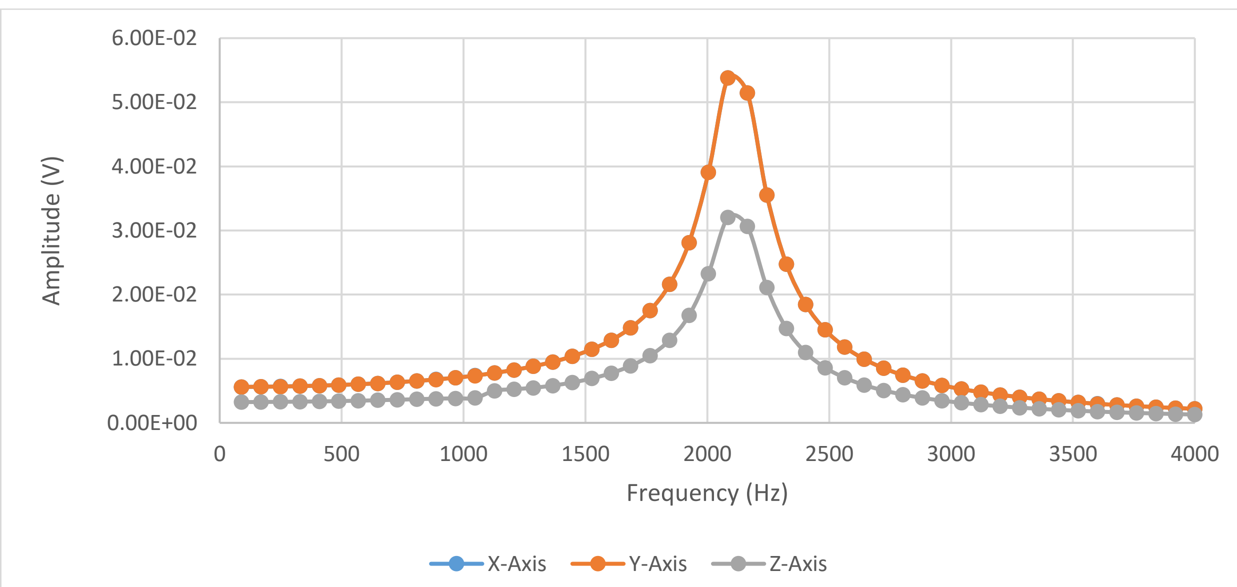

Figure 2.7. Preliminary sensor output from 1g acceleration in the x-axis and the y-axis.

Comparing the performance of an input vibration in one direction from the 1-D sensor to the 3-D sensor shows only a slight shift in the resonance peak, but no change in performance in the low frequency range (< 1000 Hz), as shown in Fig. 2.8. This is favorable as both designs will be able to characterize vibration events within nuclear power plants.

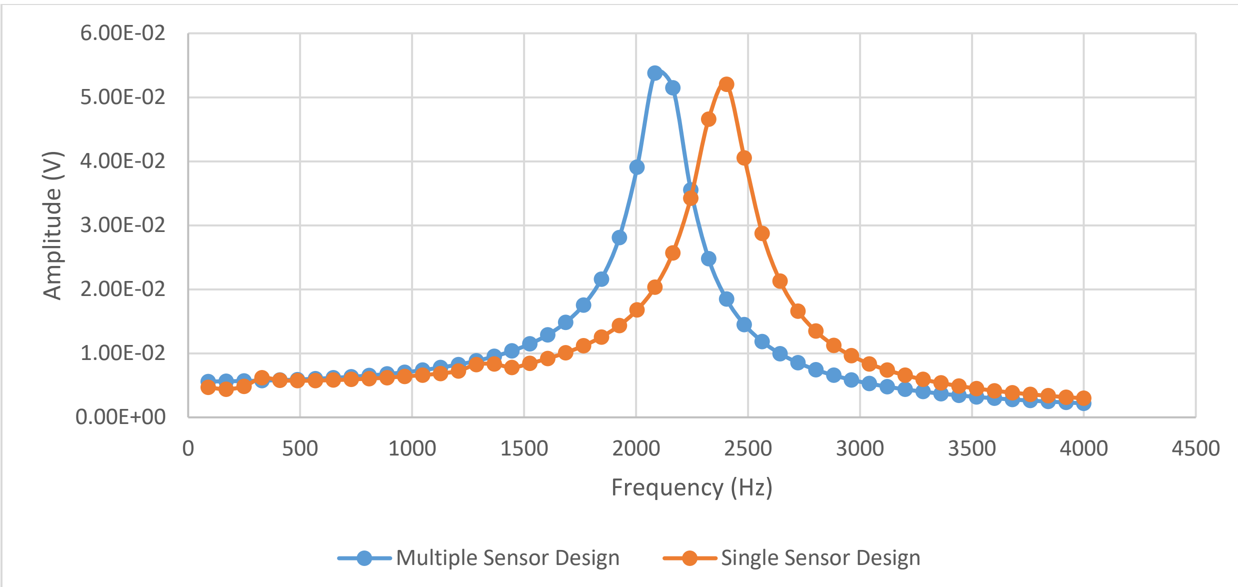

Figure 2.8. Comparison of the low frequency performance of the 1-D to 3-D sensor designs for an input acceleration of 1g in the x-axis.

Baseline noise in sensors that should not be experiencing a vibration was able to be removed by improving the optimization within the simulation software corresponding to the location of the actual sensor placement. The result showed a drastic improvement in the low frequency region, as seen in Fig. 2.9, the y-axis and z-axis showed no response to a 1g acceleration in the x-axis after the optimization. The difference between the measured signal from the x-axis and the other two axis is sufficient to determine the intensity of the incident vibration signal. The value can be seen in Table 2.2 which shows an order of magnitude difference between the signals in the low frequency region. The result of a 1g acceleration in all directions, shown in Fig. 2.10, shows similar performance from each individual axis, while the sensitivity of each direction in Table 2.3 is also similar to the x-axis reported in Table 2.2.

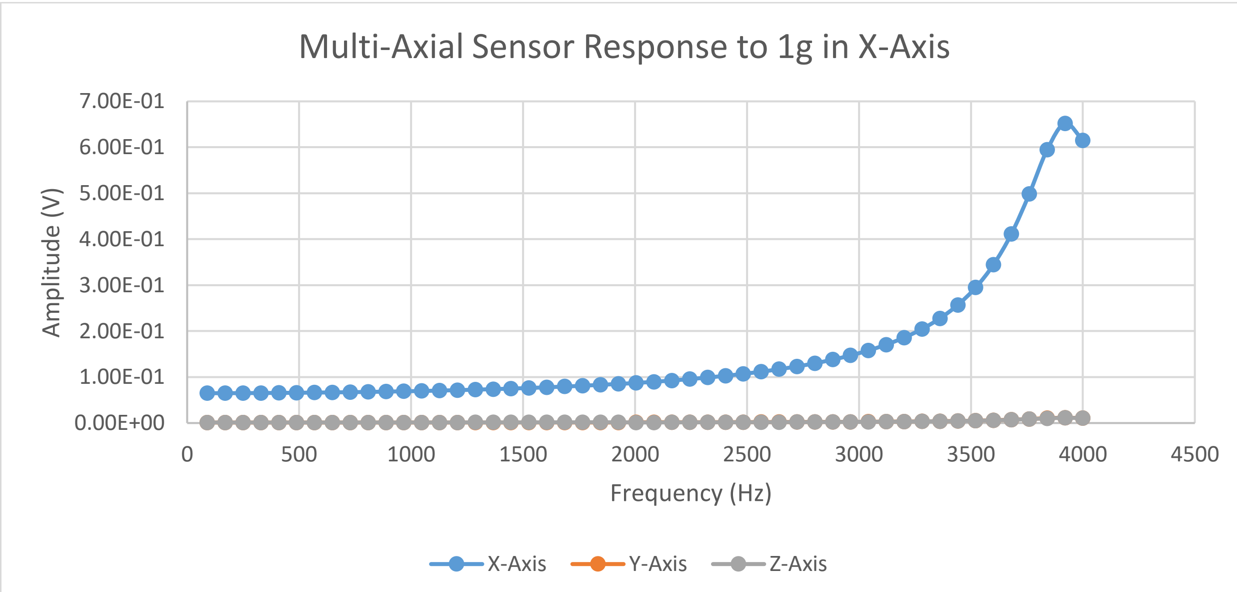

Figure 2.9. Improved performance of the multi-directional sensor in the low frequency region.

Table 2.2. Maximum amplitude response for each direction in the low frequency region from an input of 1g acceleration in the x-direction.

Max Sensitivity (mV/g)	
X-Axis	69.83
Y-Axis	1.15
Z-Axis	1.28

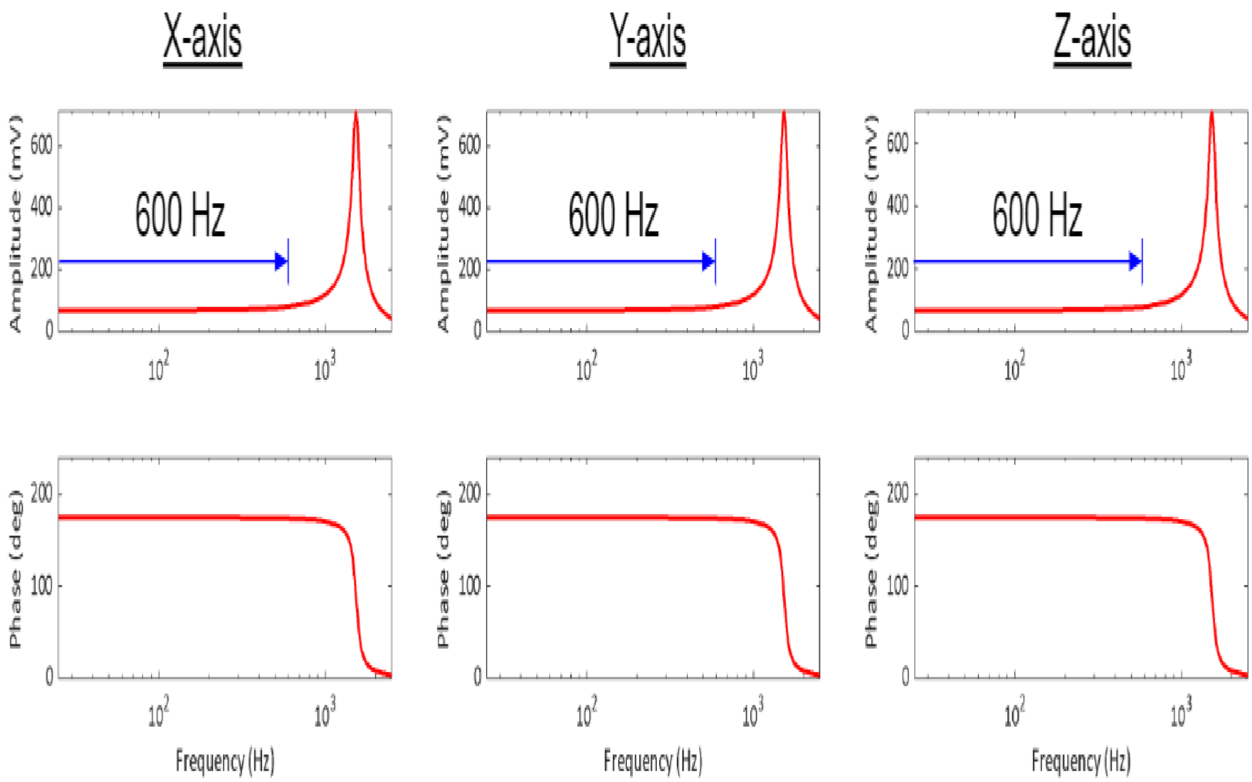

Figure 2.10. Performance of the multi-axial sensor when each axis is subjected to 1g acceleration.

Table 2.3. Sensitivity of each sensing element when exposed to a 1g acceleration.

Sensitivity (mV/g)	
X-Axis	73.9
Y-Axis	73.9
Z-Axis	72.8

2.4.2 Experimental Results

The preliminary tests were performed by attaching the multi-axial sensor to the vibration shaker. The setup of the test is shown in Fig. 2.11. The output from the sensor was relayed into a charge amplifier and signal conditioner. The results of the processed signals are shown in Fig. 2.12. The different frequency regions tested showed a peak-to-peak signal of approximately 1 mV. This signal strength is extremely small, especially when compared to the simulation results. Additional analysis needs to be performed to enhance the output signal from the multi-axial sensor.

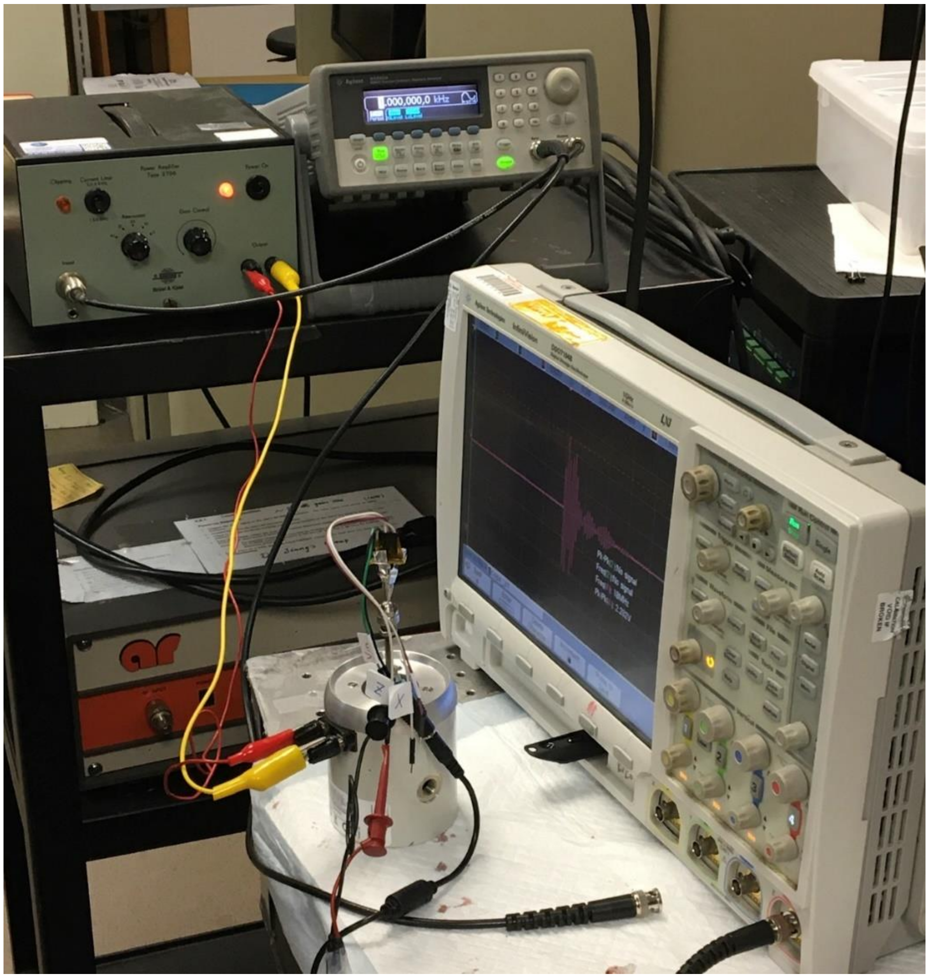

Figure 2.11. Multi-axial sensor testing setup.

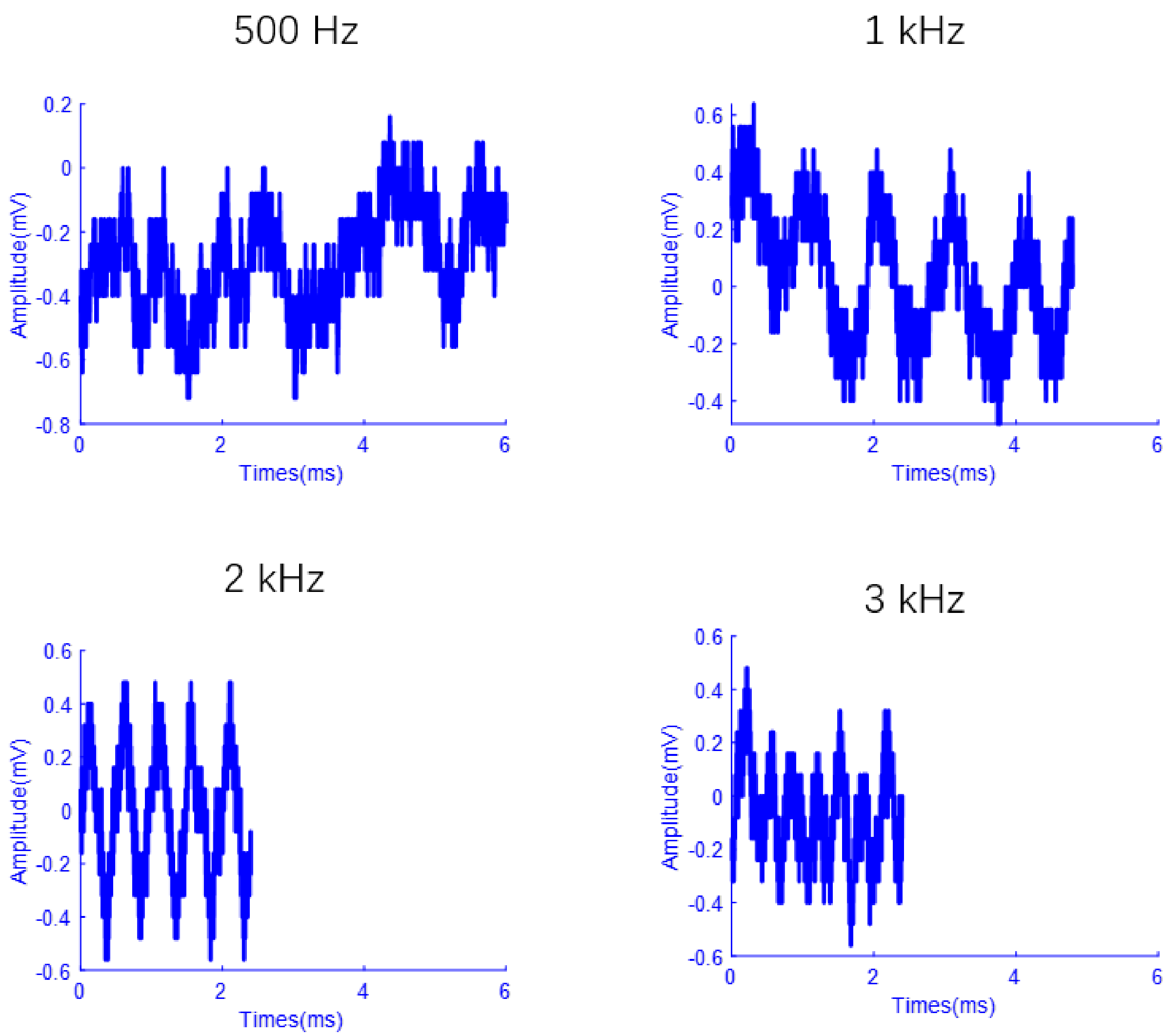

Figure 2.12. Experimental results of the multi-axial sensor of the x-axis at various frequencies.

The difference between the simulated model of the multi-axial vibration sensor and the experimental results may stem from a few different areas including issues with sensor fabrication, high electrical noise, or faulty generation of the input vibration signal. The preliminary testing of each individual axis of the sensor to measure the electrical impedance and dielectric loss, showed similar performance of each axis to the uni-axial fabricated and designed sensor. The electrical properties analysis of the isolated AlN single crystal sensing elements and the fabricated multi-axial sensor showed no indication that fabrication of the sensor was performed incorrectly; however the fabrication process of attaching the AlN single crystal to the seismic mass to ensure strong conductivity while not allowing the crystal to cause an electrical short by touching the outside wall is a delicate process. A slight connection between the two sides of the AlN crystal will either cause faulty sensor response or produce no signal at all due to an electrical short.

The testing setup, shown in Fig. 2.11, shows the output of the sensor being displayed on an oscilloscope. The output signal from the sensor passed through a charge amplifier then into a signal conditioner before being displayed on the oscilloscope. The various connections generate electrical noise. The main attributor to the electrical noise resides in the connection from the sensor to the charge amplifier as the wires connected to the sensor simply rest on the AlN single crystal while the other side of the wire needs to connect to a commercial charge amplifier, thus alligator clips are often used to ensure a strong connection. The addition of another conducive metal in the pathway of the sensors output signal results in high electrical noise that makes differentiating the signal from the noise difficult, especially with faint or weak sensitivity.

Another discrepancy between the simulated and experimental results is due to the vibration generator. The fabricated sensor rested on top of the shaker which would generate a controlled vibration. The performance of the shaker was not as consistent as would be expected. This may be due to improper operating ranges during the shaker's lifetime or general wear and tear, thus the vibration the fabricated sensor experience may not be similar to the vibration the simulation experienced. This would cause the results to be significantly different especially if the shaker was not producing strong vibrations for the sensor to sense.

There are several reasons to why the simulated and experimental results differed. As shown by a few of the reasons above, the process of fabricating the multi-axial sensor requires several carefully attached parts while the simulated model is exactly as created. The sensor signal connections also differ in the simulation compared to the experimental method as the wires generate additional electrical noise. Future iterations of the multi-axial sensor need to ensure short wires with specific attention to wire connection points. This should ensure reduced electrical noise and reduce the likelihood of electrical shorting.

2.5 Conclusions

A multi-axial vibration sensor was designed using the Ansys computer software. The simulation showed the AlN active sensing element having a sensitivity of 72 mV/g of acceleration. The working frequency range was measured to be below 600 Hz. This frequency range is perfect for application in nuclear power plants. The sensor was fabricated using methods employed by the uni-axial vibration sensor previously The materials used are the same as the uni-axial design, though the sensor utilizes three AlN sensing elements (one aligned with the x-axis, one aligned with the y-axis, and one aligned with the z-axis). The experimental results of the fabricated sensor showed small peak-to-peak amplitudes of only 1 mV. These signals are post signal conditioning, thus further refinement to reduce the effect of noise on the system or ways to amplify the magnitude of the output signal need to be employed.

2.6 References

[1] Wilson, J. S. (2005). Sensor Technology Handbook. Newnes.

[2] Partridge, A.; Reynolds, J. K.; Chui, B. W.; Chow, E. M.; Fitzgerald, A. M.; Zhang, L.; Kenny, T. W. A High-Performance Planar Piezoresistive Accelerometer. Journal of Microelectromechanical Systems, 2000, 9, 58-66.

[3] S. Zhang, X. Jiang, M. Lapsley, P. Moses, and T. R. Shrout, “Piezoelectric Accelerometers for Ultrahigh Temperature Application,” Applied Physics Letters, Vol. 96, No. 1, 013506, 2010.

[4] S. Zhang and F. Yu, “Piezoelectric Materials for High Temperature Sensors,” Journal of the American Ceramic Society, Vol. 94, No. 10, pp. 3153-3170, 2011.

[5] M. W. Hooker, “Properties of PZT-Based Piezoelectric Ceramics between-150 and 250 C,” NASA/CR-1998-208708, Lockheed Martin Engineering and Sciences Co., VA, 1988.

[6] A. Jain, A. K. Sharma, and A. Jain, “Dielectric and Piezoelectric Properties of PVDF/PZT Composites: A Review,” Polymer Engineering & Science, Vol. 55, No. 7, pp. 1589-1616, 2015.

[7] J. Liang, L. Zhang, L. Wang, Y. Dong, and T. Ueda, “Flip Chip Bonding of a Quartz MEMS-Based Vibrating Beam Accelerometer,” Sensors, Vol. 15, No. 9, pp. 22049-22059, 2015.

[8] R. T. Smith and F. S. Welsh, “Temperature Dependence of the Elastic, Piezoelectric, and Dielectric Constants of Lithium Tantalate and Lithium Niobate,” Journal of Applied Physics, Vol. 42, No. 6, pp. 2219-2230, 1971.

[9] G. Ohlendorf, D. Richter, J. Sauerwald, and H. Fritze, “High-Temperature Electrical Conductivity and Electro-Mechanical Properties of Stoichiometric Lithium Niobate,” Diffusion Fundamentals, Vol. 8, No. 6, 2008.

[10] A. V. Sotnikov, H. Schmidt, M. Weihnacht, E. P. Smirnova, T. Y. Chemekova, and Y. N. Makarov, “Elastic and Piezoelectric Properties of AlN and LiAlO2 Single Crystals,” IEEE Transactions on Ultrasonics, Ferroelectrics, and Frequency Control, Vol. 57, No. 4, pp. 808-811, 2010.

[11] Zhang, X., Zhao, S., Wang, F., Ma, Y., Wang, L., Chen, D., Zhao, C., Yang, W. (2017). Improving dielectric properties of BATIO3/Poly(vinylidene fluoride) composites by employing core-shell structured batio3@poly(methylmethacrylate) and batio3@poly(trifluoroethyl methacrylate) nanoparticles. Applied Surface Science, 403, 71–79. https://doi.org/10.1016/j.apsusc.2017.01.121

[12] G. Hayward and J. Bennett, “Assessing the Influence of Pillar Aspect Ratio on the Behavior of 1-3 Connectivity Composite Transducers,” IEEE Transactions on Ultrasonics, Ferroelectrics, and Frequency Control, Vol. 43, No. 1, pp. 98-108, 1996.

[13] H. J. Lee, S. Zhang, Y. Bar-Cohen, and S. Sherrit, “High Temperature, High Power Piezoelectric Composite Transducers,” Sensors, Vol. 14, No. 8, pp. 14526-14552, 2014.

[14] J. Streque, T. Aubert, N. Kokanyan, F. Bartoli, A. Taguett, V. Polewczyk, and O. Elmazria, “Stoichiometric Lithium Niobate Crystals: Towards Identifiable Wireless Surface Acoustic Wave Sensors Operable up to 600° C,” IEEE Sensors Letters, Vol. 3, No. 4, pp. 1-4, 2019.

[15] P. W. Krempl, “Quartzhomeotypic Gallium Orthophosphate: A New High-Tech Piezoelectric Crystal,” Ferroelectrics, Vol. 202, No. 1, pp. 65-69, 1997.

[16] T. Kim, J. Kim, R. Dalmau, R. Schlesser, E. Preble, and X. Jiang, “High-Temperature Electromechanical Characterization of AlN Single Crystals,” IEEE Transactions on Ultrasonics, Ferroelectrics, and Frequency Control, Vol. 62, No. 10, pp. 1880-1887, 2015.

[17] Park, D. Y., Joe, D. J., Kim, D. H., Park, H., Han, J. H., Jeong, C. K., Park, H., Park, J. G., Joung, B., Lee, K. J. (2017). Self-powered real-time arterial pulse monitoring using ultrathin epidermal piezoelectric sensors. Advanced Materials, 29(37), 1702308. https://doi.org/10.1002/adma.201702308

[18] Hosseini, E. S., Manjakkal, L., Shakthivel, D., Dahiya, R. (2020). Glycinechitosan-based flexible biodegradable piezoelectric pressure sensor. ACS Applied Materials & Interfaces, 12(8), 9008–9016. https://doi.org/10.1021/acsami.9b21052.s002

[19] Kim, K., Zhang, S., Salazar, G., Jiang, X. (2012). Design, fabrication and characterization of high temperature piezoelectric vibration sensor using YCOB crystals. Sensors and Actuators A: Physical, 178, 40–48. https://doi.org/10.1016/j.sna.2012.02.003

[20] Kim, S. W., Chae, S. J., Kim, D. S., Woo, J. U., Kim, E. J., Go, S. H., Eum, J. M., Kang, H. W., Han, S. H., Nahm, S. (2022). High-Power Piezoelectric Energy Harvester produced using [001]-textured (Na, k)nbo 3-based lead-Free Piezoceramics. Journal of the American Ceramic Society, 106(1), 488–500. https://doi.org/10.1111/jace.18770

[21] Kim, H., Kerrigan, S., Bourham, M., Jiang, X. (2021). ALN Single Crystal Accelerometer for Nuclear Power Plants. IEEE Transactions on Industrial Electronics, 68(6), 5346–5354. https://doi.org/10.1109/tie.2020.2992002

CHAPTER 3

REAL-TIME APPLICATION TESTING

3.1 Background

Nuclear power plants use sensors to measure multiple processes across the plant simultaneously. The Nuclear Regulatory Commission (NRC) defines required measurable parameters within a nuclear power plant as temperature, flow, pressure, neutron flux, gamma, fission product release, dust concentration, moisture, pebble burnup, confinement atmosphere chemistry, control rod position, and vibration [1]. Instrumentation that measures and monitors the parameters mentioned are often located within the reactor core, within or on the reactor pressure vessel, on reactor cooling systems, inside the steam generator, on the intermediate heat exchanger, on the gas turbine, and on the heat transport loop of the plant. Sensors are installed across nuclear power plants to ensure components operate within their set operational bounds and to monitor and regulate the operating conditions of the plant to maintain safe operation [2].

The VHTR is a Gen. IV reactor design that commercially will not be available before 2040. Testing instrumentation designed for the VHTR proves difficult since the reactor has not been constructed [3]. While designing a sensor, performance is measured by inducing controlled parameter changes and measuring the sensors response to these changes. Sensor benchmarking is typically performed under ideal conditions while sensors outfitted within a nuclear power plant will not operate with the same luxury. The operating conditions of the reactor subject sensors to harsh environments that can influence the performance of the sensors. Depending on the type of sensor in a nuclear power plant, the measured output signal could be a combination of signals. Looking at accelerometer measurements for example, the signal recorded could be a combination of variables within the power plant giving off vibration signals or micro-tremors from nature. The combination of these signals becomes complex as it is difficult to identify the major contributor to the signal. Within a laboratory setting, the signal is directly generated by a vibration shaker that can be controlled. The fabricated sensor is solely measuring the vibration output by the shaker and any electrical noise. Laboratory sensor fabrication provides benchmarking of the sensor performance and technical capabilities to ensure it can handle the requirements of the desired application, but sensor testing within the given application often leads to unforeseen increases in the complexity of measurement or data analysis. Fabricated sensors should be characterized within the laboratory setting to identify the technical capabilities of the sensor, but the sensors should also be tested in an industrial application to see how the sensor adapts to the intended application.

3.2 Objectives

In order to evaluate the sensor performance in a simulated environment, a mock-up experiment is used to induce changes on a system and have the sensor relay the information about the changes. The AlN piezoelectric vibration sensors aim to predict changes in the system due to natural effects such as earthquakes, system changes such as power increases, and external damage on the specific instruments. By developing a method to test the sensors capability of determining when system changes occur and the source of the change, the sensor can be simulated to tasks similar to those within a nuclear power plant. The preliminary changes focus on change in vibration levels due to temperature and flow rate shifts. Commercial power reactors use flow pumps to circulate the coolant to the reactor core. These pumps generate strong vibrational forces both from the actuation of these devices, but also from the flow of the water within the pipes. The location of the piezoelectric sensor can determine the intensity of the vibrational effect nearby the sensor and monitor the strength of these effects to ensure the power plant operates within set vibrational levels of these crucial plant components.

3.3 Materials & Methods

In order to assess the performance of the fabricated sensor outside of ideal laboratory conditions, a mock-up chamber was designed to simulate system parameters that affect sensor performance. The goal of this system is to measure and control parameters that exist in operational nuclear power plants. The Room-Temperature Mock-Up Experiment (RTME) was designed to perform sensor characterization in real-time. Nuclear power plants use instrumentation and controls to manage every aspect of the power plant operations. A few examples of areas where I&Cs are used are in monitoring the coolant flow throughout the power plant. The reactor pressure vessel must maintain a nominal liquid level in order to ensure the control rods are covered. Having a liquid level too low or too high can lead to serious consequences, thus I&Cs focus around ensuring a proper balance of the coolant entering the system. The designed mock-up, shown in Fig. 3.1, measures the temperature of the liquid within the main chamber. This would be useful to monitor if steam is being produced. The flow rate of the inlet coolant stream is measured by a flow sensor that would be able to ensure the rate that water is being converted to steam matches the inlet. This will ensure the liquid level remains at a constant threshold. Vibration measurements can show structural damage within the system. By measuring the vibration of key locations on the mock-up system, detailed information into the stability of the coolant pipes can be determined. The mock-up utilizes the liquid level, temperature, flow rate, and vibration measurements to monitor a simulated version of what would be the coolant stream in a nuclear power plant. The simulated system shows the Mock-up tank which circulates a liquid solution through a series of flow pumps. The gate values ensure that the flow rate reentering the tank can be changed quickly. The inside of the tank uses a ceramic heater to control the temperature of the circulating fluid. The control parameters of the RTME are shown in Table 3.1 below. A flow meter is used to measure the flow rate of the liquid circulating throughout the chamber. By opening and closing the flow control valves, the flow rate is changed, thus being shown by the output of the flow meter. The ceramic heater is accompanied by a thermocouple which is set inside of the steel chamber to measure the temperature of the circulating liquid.

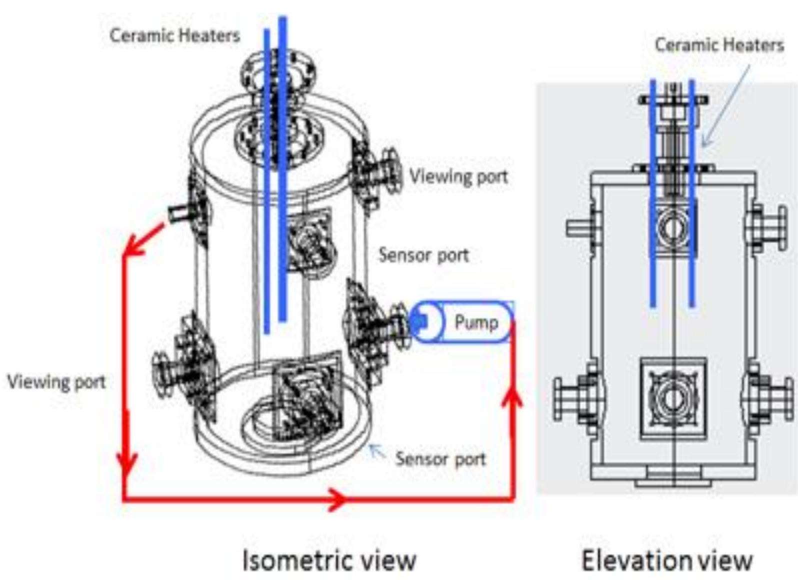

Figure 3.1. Rendered diagram of the Room-Temperature Mock-Up Experiment.

Table 3.1. Design specifications of the Room-Temperature Mock-Up Experiment.

Control Parameters	**Sensor**	**Range**
Temperature	KLC Temperature Controller and Thermocouple	20 °C to 100 °C ± 1 °C
Flow Rate	OMEGA In-Line Flow Meter	0 gal/min to 5 gal/min ± 0.1 gal/min
Liquid Level	Chamber wall markings	15 in to 40 in ± 1 in
Vibration	AlN Piezoelectric Accelerometer	9.2 pC/g sensitivity, up to 600 Hz

The constructed RTME, shown in Fig. 3.2, utilizes a stainless steel tank with multiple outlet ports to act as inlets and outlets. The preliminary flow consists of using water was the liquid, thus PVC piping is used as water will not harm the pipes. Two circulating loops are constructed with piping, flow control valves, and pumps attached to each loop. The ideology behind the RTME involves acting as a basic reactor system in the sense that a sensor could measure the changes of various controllable system parameters. By placing the sensor above the inlet flow port, the sensor can measure the changes in vibration level associated with changes in flow rate. The liquid level within the chamber is monitored by visual inspection of markings within the walls of the chamber. The visual inspection occurs by utilizing the side viewing ports to see the wall markings. Typically, nuclear power plants will utilize level buoys to measure the liquid level within the tank without needing electronics. In order to control the liquid level, additional liquid would need to be added or removed by utilizing the chamber side ports. The system provides insight into the performance of the sensor in applications with unknown vibrations. The sensor testing using this system allows for the practical application response of the sensor to be tested.

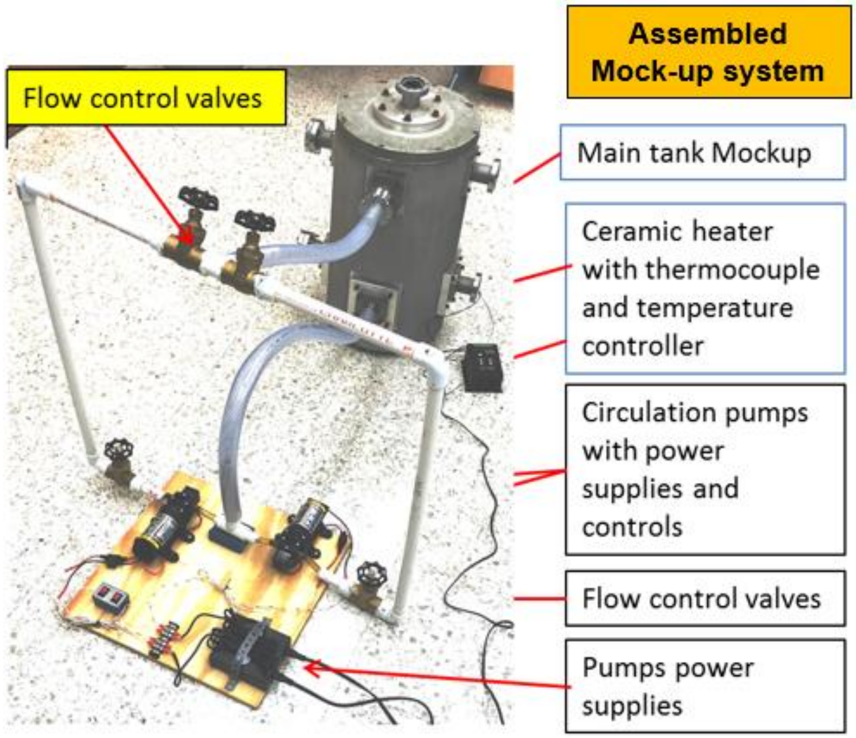

Figure 3.2. Schematic of the Room-Temperature Mock-Up Experiment.

The fabricated sensor was designed using the design mentioned in Chapter 2 with AlN as the sensing material. The working range of the fabricated accelerometer is up to 600 Hz. The sensor output passed through both a charge amplifier and a signal conditioner (using the same specifications mentioned in Chapter 2), as shown in Fig. 3.3. The output signal was then fed into a data communication board which transmits the data wirelessly to the computer where the data is processed and transformed. The sensor output was converted to power based on the following equation:

$$P_{out} = 0.036 * V_{in} + 2.5 \tag{3.1}$$

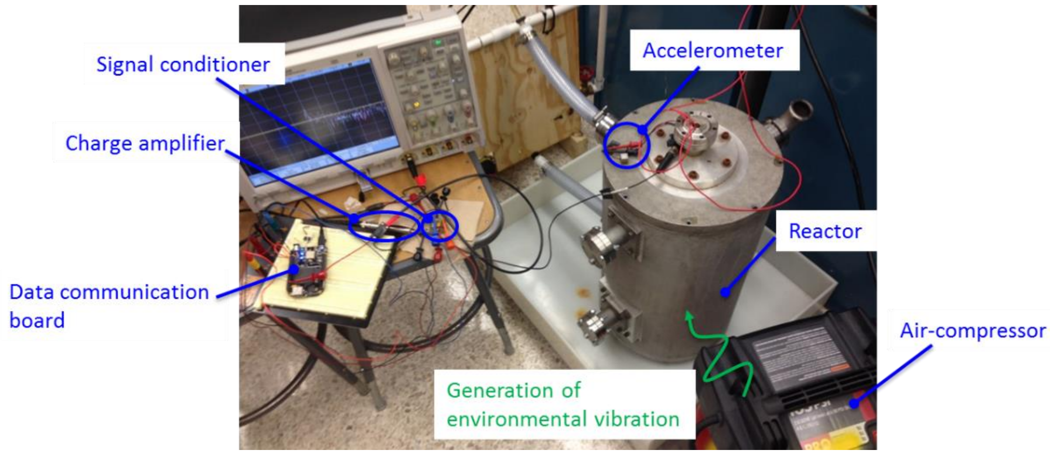

Figure 3.3. The Room-Temperature Mock-Up Experiment being used to simulate vibration data for the sensor.

3.4 Results & Discussion

Using the RTME, the sensor was placed directly above the inlet flow port. The sensor response was measured as shown in Fig. 3.4 (a-b) at flow rates corresponding to 50% flow (half-flow) and 100% flow (full flow). When the output signal is shown in the time domain, the changes in the signal are difficult to observe due to flow rate manipulation. In order to extract system information from the sensor response, the data must be processed.

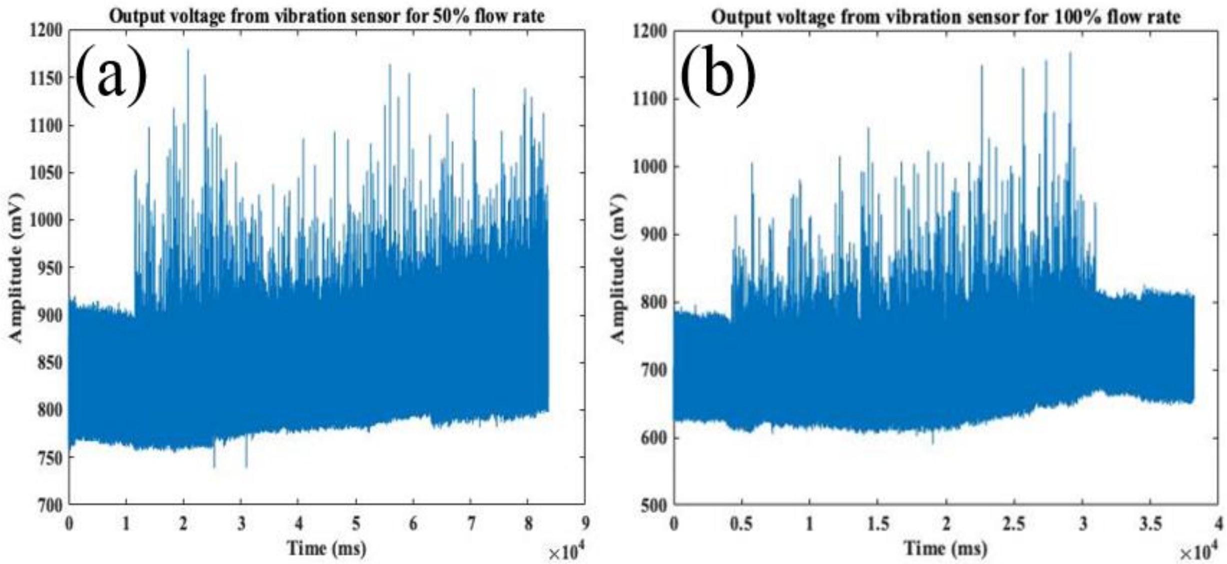

Figure 3.4. Sensor output signal measuring the change in flow rate at 50% flow rate (a), and 100% flow rate (b).

When the signal is processed in terms of the power vs frequency domain , the change in the signal as a function of flow rate can be observed. The power shown is the amplitude of the g-force applied that is calculated by performing a FFT on the output sensor signal. The signals contained a lot of electrical interference occurring around the 50-60 Hz range, thus extracting the information specifically pertaining to the vibration sensor signal proved challenging. The peak power in Fig. 3.5 (a) at 50% flow rate can be observed at 9.375 dB while the peak power in Fig. 3.5 (b) is observed at 12.18 dB. The slight improvement in the amplitude of the sensor response shows the proper trend as a function of measuring the flow rate, but additional characterization of the active sensing material and signal processing electronics needed to be performance to ensure the result is strictly a result of the sensor and not background interference.

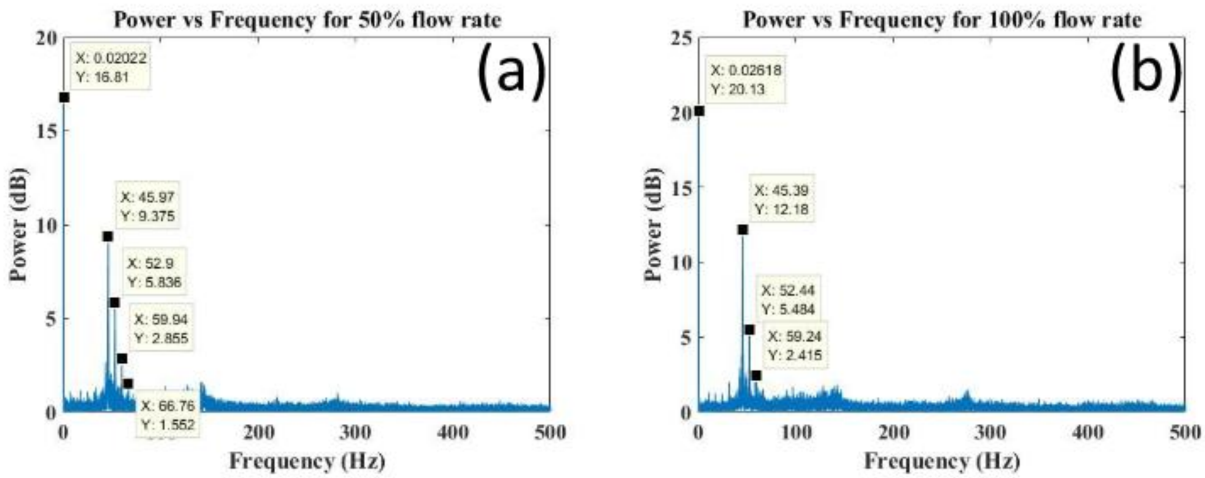

Figure 3.5. Changes in power amplitude as a function of flow rate operating at 50% flow rate (a), and 100% flow rate (b).

The RTME was the first steps in testing the actual sensing element outside of traditional laboratory tests. It also presented the opportunity for the communication network and sensor to interact allowing for the entire proof-of-concept to be demonstrated. The applicability of non-intrusive wireless vibration sensors rests on the idea that the sensor can accurately capture the system data while the communication network can process and transmit the data without any interference affecting the signal. The results of the communication network testing, shown in Fig. 3.6, prove the communication system was successfully able to collect the vibration response data in as few as 800 samples. This test was performed at a sampling rate of 57 kHz based on the Nyquist criterion of the sampling rate being at least twice as large as the highest frequency. The communication test was an excellent first demonstration of the sensor and wireless communication system working together to output the captured information in only 800 samples [4]. The number of samples is important because the required number of samples required to process and output the data should try to be minimized as the data is transmitted wirelessly. The smaller the number of samples, the smaller the data packet, which means less delay due to transmission.

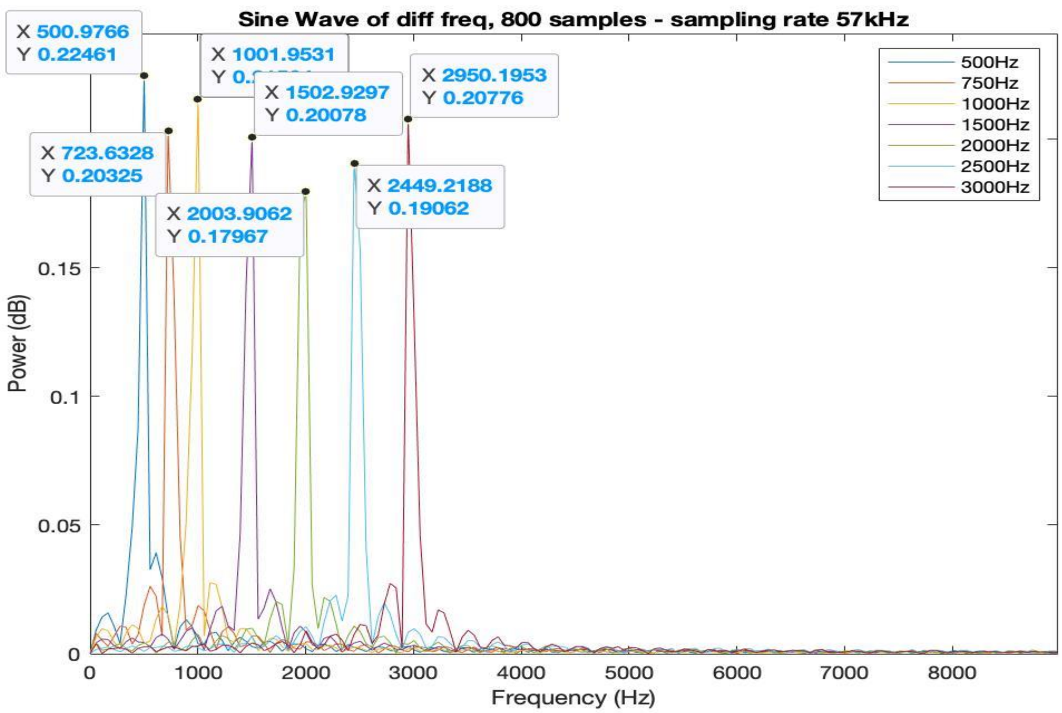

Figure 3.6. Wireless communication network data output of vibration sensor located on the RTME.

3.5 Conclusions

The RTME showed the difficulty in predicting system information without conditions or processed data. The sensor was able to determine that an increase in vibration occurred when the flow rate was increased, but the process of determining that the vibration sensed was solely a result of the flow rate change and not a combination of multiple factors requires signal processing. The signal contained a lot of electrical interference, thus signal processing must be done to ensure these factors do not degrade the sensors data. The RTME showed the complexities of optimizing a sensor array for use in a nuclear power plant, and the RTME occurs at room temperature without almost no environmental concerns on the sensor or active sensing element, thus the optimization becomes even more challenging in a nuclear power plant application. The tests show the sensor is able to gather information about systems in real-time; however, the output from the sensor must be improved to ensure the data is solely from actually occurring vibrations. The RTME showed a few problems associated with the sensor output that grow even more difficult when placed in a harsh environment such as a nuclear power plant. In order to ensure the sensor and active sensing element can survive the harsh environment to provide reliable and accurate vibration data, additional characterization work was done focusing on the effects of radiation, temperature, and corrosion.

3.6 References

[1] Nuclear Regulatory Commission. (2020, June 5). Digital Instrumentation and Control. Nuclear Reactors. Retrieved from https://www.nrc.gov/reactors.html

[2] Korsah K., Instrumentation and Controls in Nuclear Power Plants: An Emerging Technologies Update. U.S. Nuclear Regulatory Commission, Office of Nuclear Regulatory Research, 2009.

[3] Department of Energy. (2021, April 12). 3 Advanced Reactor Systems to watch by 2030. Office of Nuclear Energy. Retrieved from https://www.energy.gov/ne/articles/3-advanced-reactor-systems-watch-2030

[4] Balagopal, Bharat, et al. High Temperature Embedded/Integrated Sensors (HiTEIS) for Remote Monitoring of Reactor and Fuel Cycle System. 2019, pp. 1–43.

CHAPTER 4

EFFECT OF RADIATION ON SENSOR MATERIALS AND PERFORMANCE

4.1 Background

The developed vibration sensors will be non-intrusive, thus the sensor can be fitted to any location outside of the reactor. The location of a specific sensor will vary depending on the desired information. It is almost certain that a sensor will be fitted to the outside of the reactor pressure vessel (RPV). Since the RPV is the closest location relative to the reactor core, it should contain the highest level of radiation effects, which could impact the performance and integrity of the sensor. The RPV is several feet thick, thus it can be assumed that only gamma-rays will be able to penetrate the thick steel [1]. For the purpose of the radiation studies, only the effects of gamma-rays on sensor materials was investigated as this fits the application of the sensing technique.

4.1.1 Radiation Damage & Effects

When high-energy radiation passes through a material, interactions occur within the lattice that can impact the stability of the material. The energetic particles cause damage within the lattice by colliding with atoms, thus transferring enough energy through these collisions, allowing the atoms to break their bonds [2]. The broken bonds allows for the formation of defects within the lattice of the material, thus inducing radiation damage. Within a nuclear reactor, there are several different types of radiation sources capable of inducing various changes in material properties such as neutrons and fission fragments. These types of particles can induce significant microstructural changes in reactor materials, causing their performance to degrade or change over time as a result from radiation exposure. Intense radiation can cause the formation of vacancies, interstitials, impurities, and depleted regions within a material. Gamma rays are capable of causing radiation damage, but there is a stark difference between the levels of damage caused by gamma rays and those by neutrons and heavy particles. The level of radiation damage is measured in displacements per atom (dpa), which shows the impact an incident neutron or gamma ray can have on the lattice of a material. The higher the dpa, the more severe the radiation damage will be. The damage produced is often proportional to the neutron flux, temperature and irradiation time [3]. Material exposure to irradiation can cause alterations to the microstructure of materials, thus the materials physical properties. Heavy particles, such as neutrons and fission fragments, can cause significant microstructural damage to materials. Forms of radiation damage caused by heavy particles include vacancies, interstitials, voids, and impurities [2].

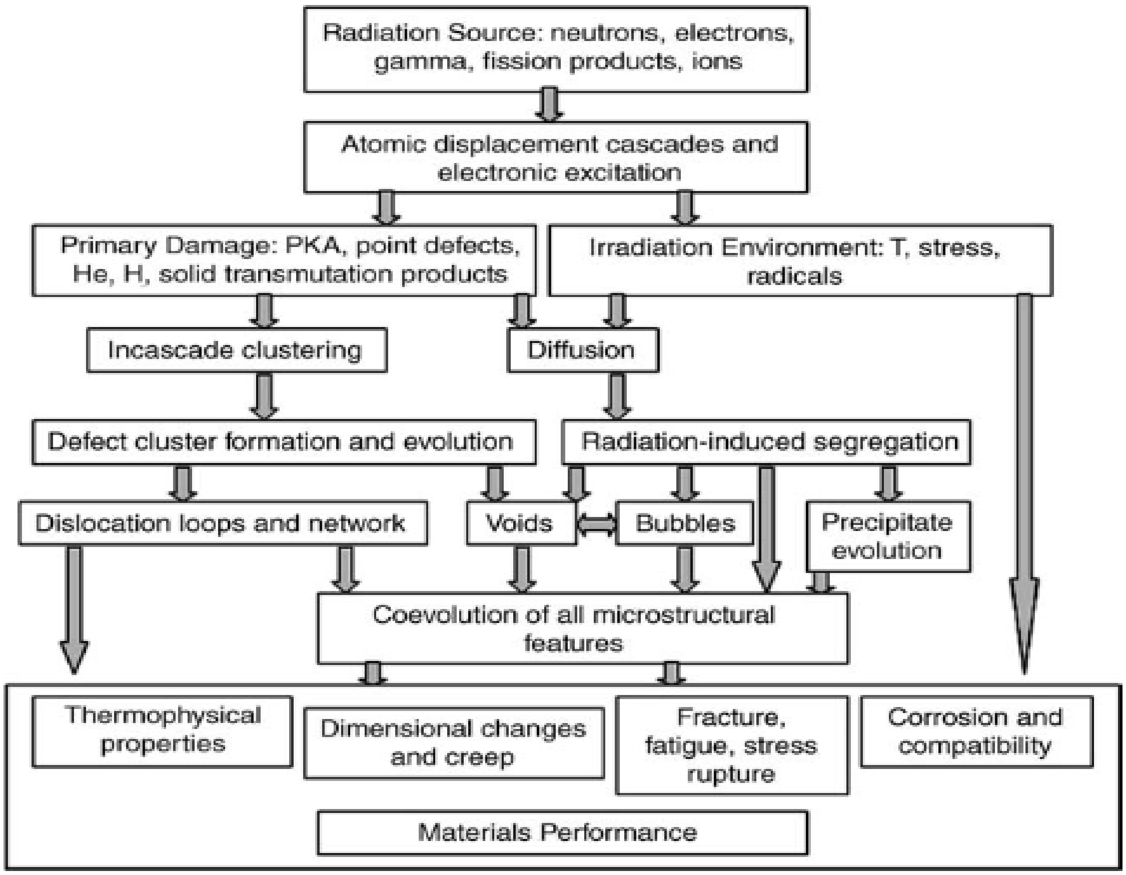

Figure 4.1. Various types of radiation damage and the effects on materials [2].

4.1.2 Radiation Induced Segregation

Several effects are the result of radiation damage within the material. At elevated temperatures, a commonly occurring result of radiation exposure leads to radiation-induced segregation (RIS). RIS causes alloy elements to segregate especially around surfaces, near grain boundaries, voids and dislocations [4]. The segregation of the alloyed elements can cause mechanical properties to degrade and properties across a material to become non-uniform, making them undesirable for nuclear power plant applications. RIS is a serious problem within the nuclear field that can be tested following irradiation to ensure materials maintain stability after radiation exposure at high-temperatures. RIS causes homogeneous alloys to become heterogeneous, significantly altering the material performance across the material. Special attention about the effects of RIS occurs in alloys containing chromium that is often used to improve corrosion resistance. The segregation of the chromium to one part of the material increase the materials susceptibility to degradation due to corrosion.

4.1.3 Radiation Hardening and Embrittlement

Radiation can cause the strength of certain alloys to increase, thus decreasing the ductility of the material. There are several defects that can cause radiation hardening to occur including vacancies and self-interstitial atoms, impurities, and dislocations [2]. The interaction between the material lattice and incident particles causes the formation of defects such as dislocations that entangle the lattice, thus increasing the hardness of the material. The same mechanisms can also lead to material embrittlement. Radiation damage leading to embrittlement lowers the threshold energy required to cause material fracture. Both radiation hardening and embrittlement alter the physical performance of materials after radiation exposure. Within a sensor, this could cause the sensing material or the sensor housing to fail. This would destroy the sensor and depending upon the location of the sensor could lead to sensor components entering the reactor.

4.2 Objectives

Understanding the performance of materials when exposed to radiation is measured must occur prior to permitting a material to be used within a nuclear reactor. As shown previously, radiation can have several different effects on a material affecting various material properties that impact the performance of the material. Material testing to understand the performance of a material before and after irradiation must occur prior to licensing any sensor to nuclear power plant applications. The testing also provides insight into the stability and lifetime of the sensor within a nuclear power plant environment. The objective of this study aims to identify the effects of irradiation on the aluminum nitride sensing elements and on a fabricated sensor. The effects of gamma irradiation can be studied by irradiating samples and performing materials characterization to study if prolonged gamma exposure can effect the surface topography and electrical performance of the sensor materials. The effects of heavy ions must be studied as the radiological environment that a nuclear power plant sensor may be exposed to would contain both gamma and neutron sources. Both of these particles can damage the sensor by altering the mechanical performance of the sensor or causing failure. By understanding the mechanism of these different types of particles, the performance of the sensor can be studied within a nuclear power plant environment.

4.3 Materials & Methods

In order to study the effects of radiation of piezoelectric sensing materials, samples of the single crystal AlN sensing element were irradiated using a Co-60 gamma source using the NCSU facilities. Samples were irradiated for either one or two months to simulate low dose of gamma exposure experienced by sensors placed on the outside of the reactor pressure vessel. At any location other than the RPV wall, the dose accumulated by the AlN sensing material will be lower, thus material analysis was performed using the location of the highest dose. The AlN samples irradiated for 1 month received an accumulated dose of 9.2 kGy and the 2 month samples received an accumulated dose of 19.3 kGy. Material characterization of the samples occurred both pre and post irradiation to compare the effects of radiation. The characterization was performed using the FEL Verios 460L Scanning Electron Microscope (SEM) at the NCSU AIF to study the surface topography of the samples. Additionally, compositional analysis was performed using Energy-Dispersive X-ray Spectroscopy (EDS) attached to the SEM at the AIF. In order to assess the sensor response to radiation, a fabricated sensor, including both the sensor housing and the AlN active sensing element, was placed within the Co-60 gamma unit for 1 month until an exposure dose of 11.2 kGy was achieved. The sensitivity of the sensor was measured both pre and post irradiation.

Investigation into the effects of neutron damage was performed using SRIM (Stopping and Range of Ions in Matter) and TRIM (Transport of Ions in Matter) programs to simulate a heavy ion beam of 14 MeV protons. The SRIM/TRIM codes are Monte Carlo-based solvers to simulate the collision of ions. The program is employed to simulate the effect of a 14 MeV monoenergetic beam of hydrogen at angles of incidence of 0° (perpendicular to the surface) and 89° (parallel to the surface) of the fabricated vibration sensor using Inconel 601 as the housing material. The relationship between angle of incidence and penetration depth will be investigated.

4.4 Results & Discussion

The SEM image shown in Fig. 5.2 shows the sample before and after radiation exposure. The surface topography looks similar, thus it can be concluded that the dose of 9.2 kGy acquired after one month has no effect on the AlN crystal. In order to observe the effects such as radiation induced segregation, the EDS analysis, shown in Table 4.1, identified that the observed sample is mostly the gold coated layer on the AlN crystals. As the nitrogen is not very conductive, it is hard for the EDS to observe its presence when the composition of gold is high. Analysis on an AlN side without gold deposition would need to be performed to observe the effect of radiation on the nitrogen composition. From these EDS results, it can be concluded that the radiation dose exposure over one month has no effect on the composition of the gold plated AlN crystals [5].

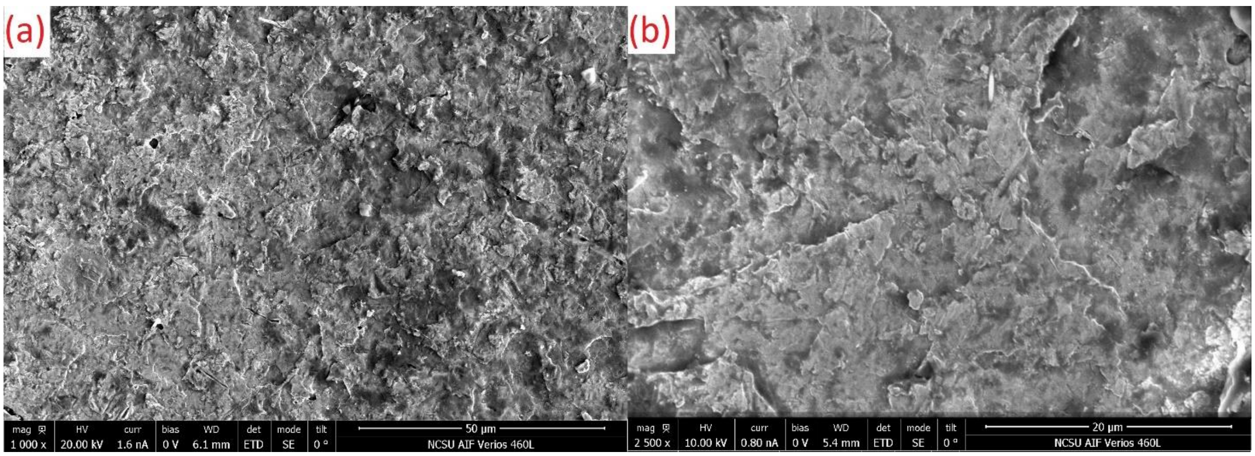

Figure 4.2. SEM image of gold plated AlN crystal before irradiation (a) and after 1 month of irradiation (b).

Table 4.1. EDS analysis of gold plated AlN crystal before irradiation and after 1 month of irradiation.

	Before Irradiation (wt%)	**After Irradiation (wt%)**
Au	89.69	99.3
Al	10.31	0.7
N	0	0

The SEM images shown in Fig. 5.3 show the AlN samples before and after radiation exposure. The majority of the surface topography looks similar, thus it can be concluded that the dose of 19.3 kGy acquired after two month has no effect on the AlN crystal. The surface microstructure is unaffected by the dose values accumulated. The EDS analysis shown in Table 4.2 identified that the measured sample is mostly the gold coated layer on the AlN crystals. From these EDS results, it can be concluded that the radiation dose exposure over two month has no effect on the composition of the gold plated AlN crystals [5]. In order to observe the effect of radiation on AlN single crystals, the samples would need to be exposed for a much longer time or a stronger dose should be used. Further analysis of the AlN response to radiation is not required as the AlN crystals will be housed within the sensor structure located outside the RPV. Since the sensors are located outside of the RPV, the walls provide sufficient shielding that the sensors should not experience high gamma exposures.

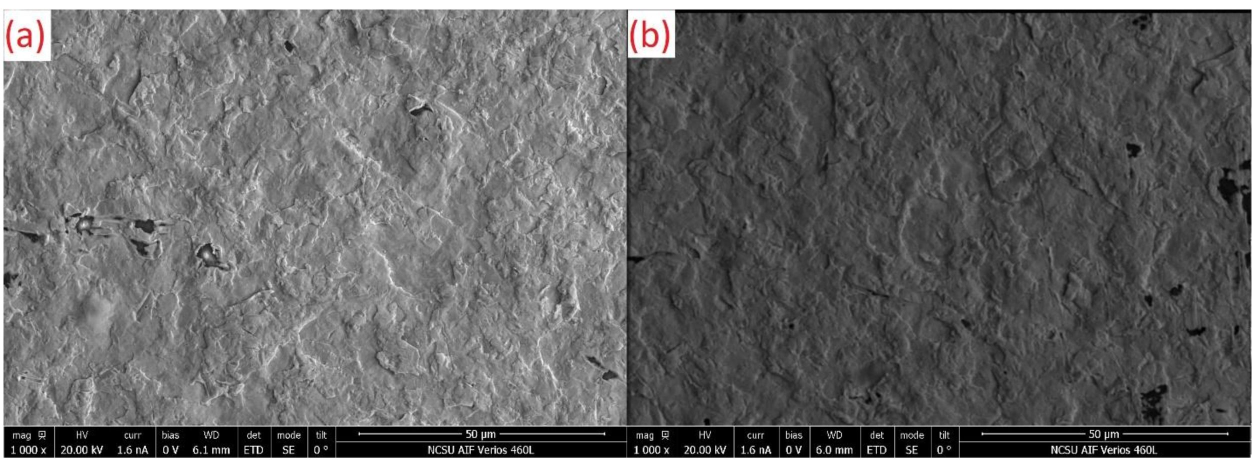

Figure 4.3. SEM image of gold plated AlN crystal before irradiation (a) and after 2 month of irradiation (b).

Table 4.2. EDS analysis gold plated AlN crystal before irradiation and after 2 month of irradiation.

	Before Irradiation (wt%)	**After Irradiation (wt%)**
Au	90.00	90.26
Al	10.00	9.74
N	0	0

The initial sensitivity of the sensor, shown in Fig. 5.3, was determined to be 9.2 pC/g ± 0.47 pC. The results of the sensitivity analysis following irradiation are shown in Fig. 4.4 below. Following the irradiation of the sensor, almost no change in the sensitivity was observed. A linear behavior was still observed with roughly the same sensitivity of 9.2 pC/g. Thus, it can be concluded that the radiation dose of 11.2 kGy did not influence the performance of the sensor [6]. This result is solely considering the effect of gamma irradiation on the sensor as other forms of radiation (neutron, alphas, and betas) are expected to be shielded by the reactor walls [1].

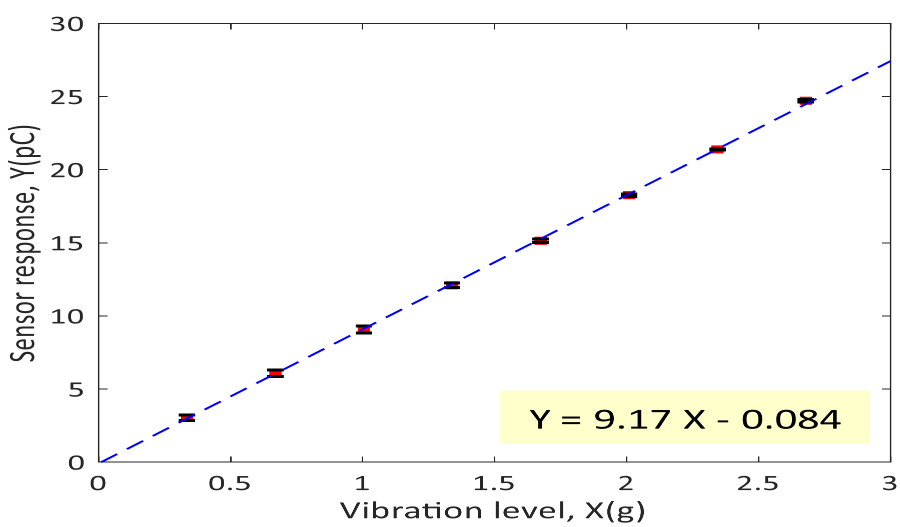

Figure 4.4. Linear output of the sensor at 1000 °C and 200 Hz excitation to determine the sensor sensitivity.

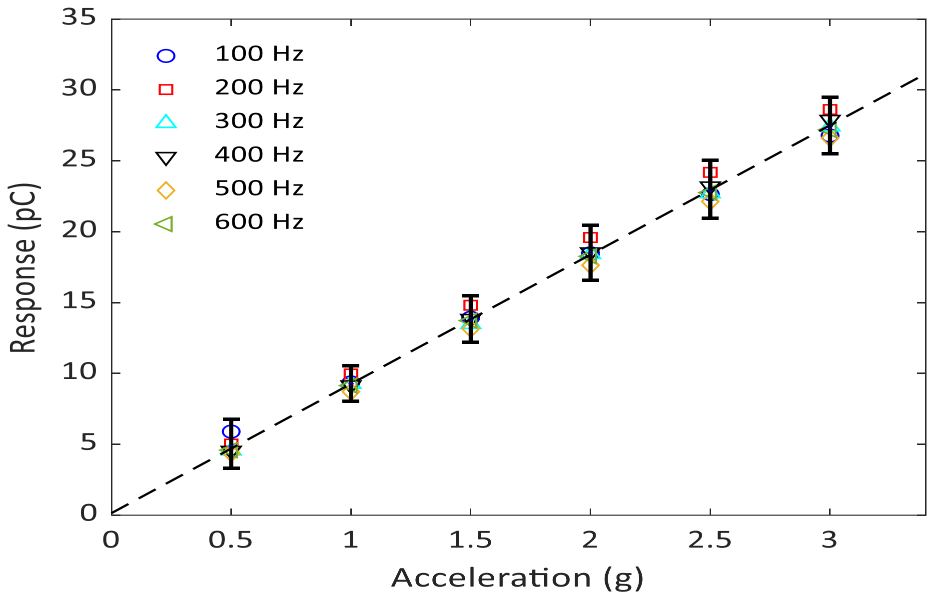

Figure 4.5. Accelerometer sensitivity analysis after irradiation using a Co-60 gamma source to achieve a dose of 11.2 kGy.

Simulation into the effects of heavy ions (protons/neutrons) on the fabricated structure revealed that the penetration depth of the monoenergetic 14 MeV hydrogen ion heavily depends on the angle of incidence. The particle distribution at an angle of incidence of 0° is shown in Fig. 4.6. The angle of incidence corresponding to 0° indicated the 14 MeV beam is perpendicular to the target layer of Inconel 601. The penetration depth at an angle of incidence of 0° is 446 µm. The target damage corresponding to an angle of incidence of 0° is shown in Fig. 4.8 (a). The 14 MeV beam is shown to completely penetrate the top 200 µm of the Inconel 601 layer of the sensor housing material. The particle distribution at an angle of incidence of 89° is shown in Fig. 4.7. At an angle of incidence of 89° (parallel to the Inconel surface), the penetration depth is 22.4 µm. The target damage corresponding to an angle of incidence of 89° is shown in Fig. 4.8 (b). The 14 MeV beam is shown to only penetrate part of the outer Inconel layer of the sensor housing material.

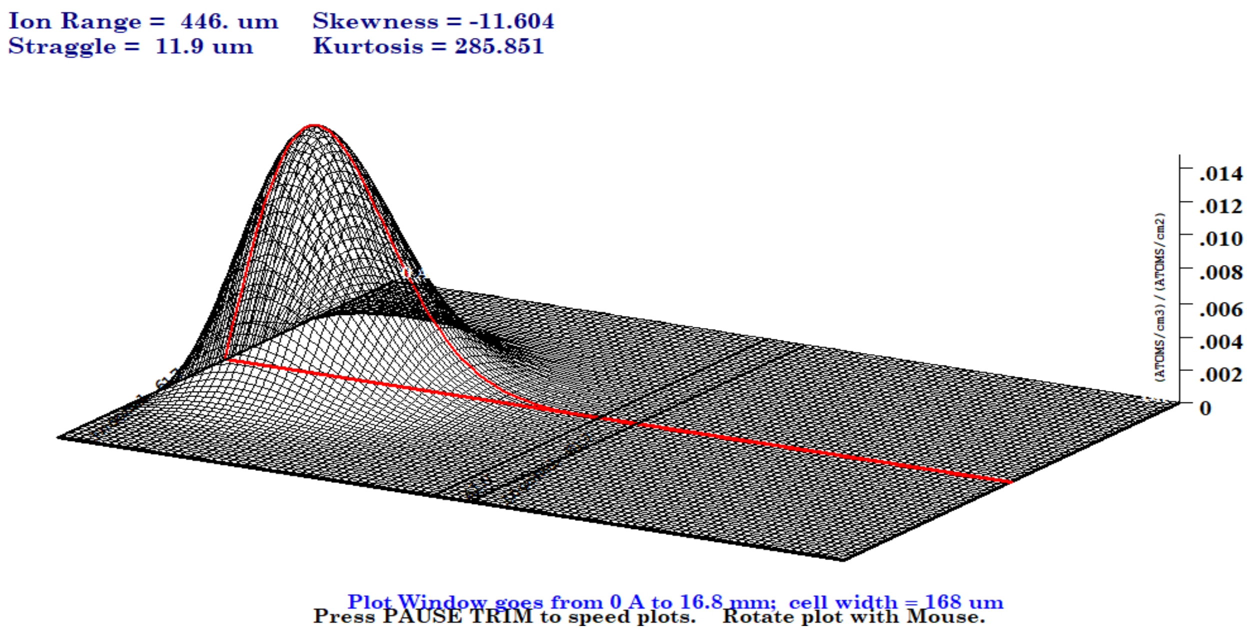

Figure 4.6. Particle distribution on Inconel 601 at 0° incidence.

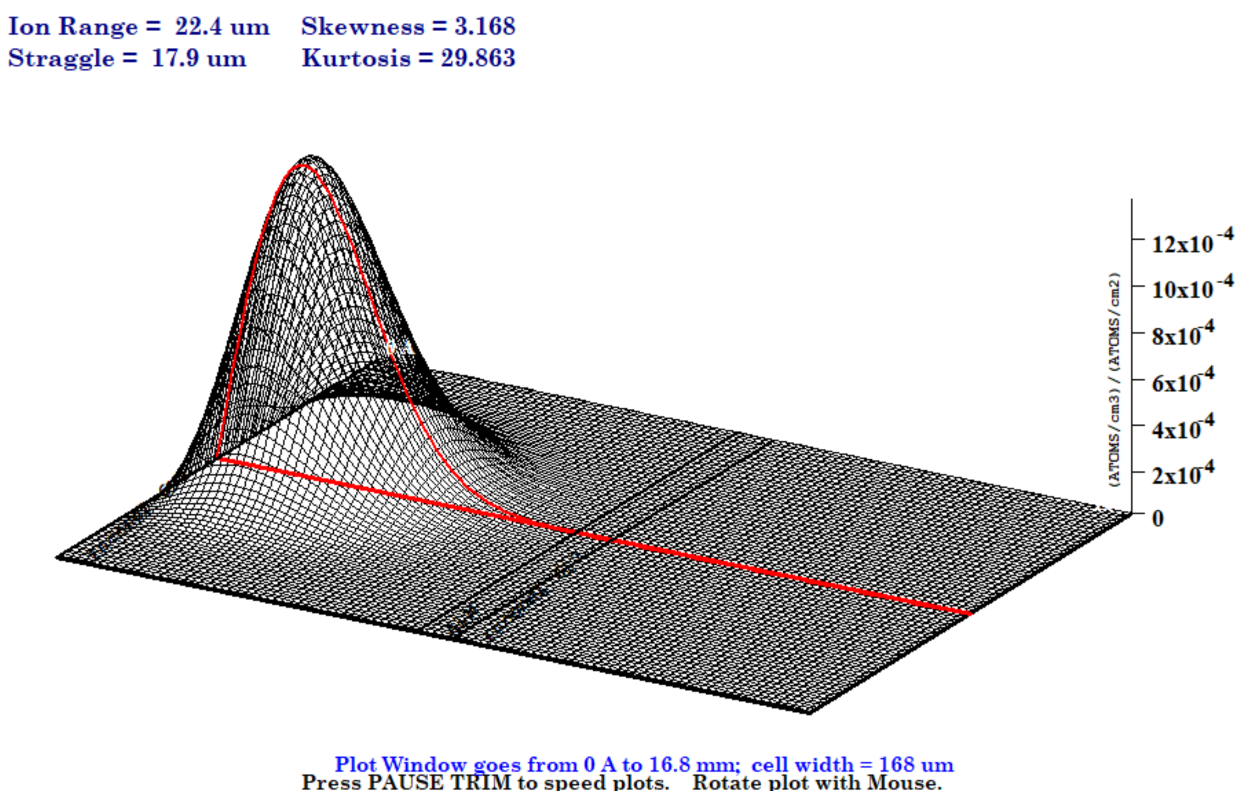

Figure 4.7. Particle distribution on Inconel 601 at 89° incidence.

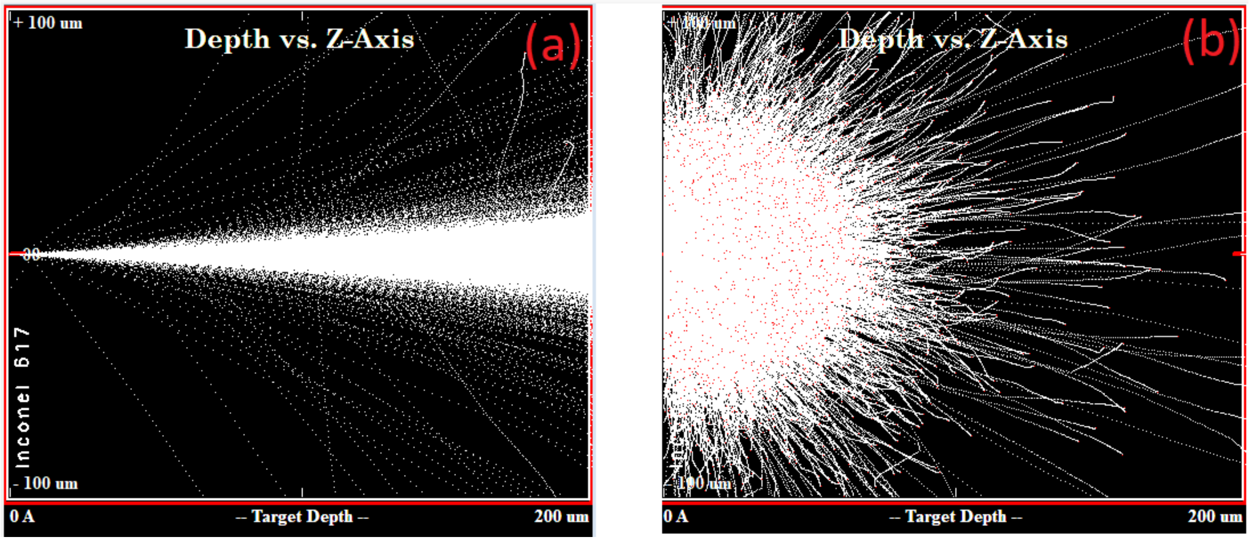

Figure 4.8. Target damage from particle impacts at angles of incidence of (a) 0° and (b) 89° for Inconel encountering a 14 MeV ion beam.

4.5 Conclusions

By placing the sensors on the outside wall of the RPV, the active sensing material would experience the highest level of exposure. In order to study the effect of radiation on the AlN sensing material, samples of AlN single crystals were exposed to a Co-60 gamma source for 1 month and 2 months. Material characterization of the samples was performed using an SEM with EDS functionally. Characterization was performed both pre and post irradiation to study the effect of radiation was studied both pre and post irradiation on the surface topography and the composition of the samples. The SEM results showed that the surface was free from any defects or inclusions formed as a result of radiation exposure. The EDS composition analysis showed that the gold-plated electrode layer maintained its integrity regardless of the irradiation time. The gamma-ray exposure on AlN single crystal samples for piezoelectric sensors did not cause any noticeable materials topography changes or composition changes, thus the AlN sensing elements will maintain their functionality in the nuclear power plant environment. The sensor irradiation tests showed that the sensor still maintains its sensitivity despite being irradiated, thus the sensor materials and design are favorable for use within nuclear power plant applications as they perform well with radiation exposure up to 20 kGy. Simulation experiments using a 14 MeV monoenergetic hydrogen beam showed that the incident angle of the beam effects the penetration depth of the particles. The beam perpendicular to the surface of the Inconel 601 target experienced the largest penetration depth of 446 μm while the beam parallel to the surface experienced a penetration depth of 22.4 μm. The beam parallel to the surface showed a much wider array of target damage, yet it did not penetrate as far. The beam perpendicular to the surface showed a thin beam penetrating deep into the Inconel 601 surface. Using Inconel 601 as the sensor housing material provided sufficient shielding of the AlN single crystals that act as the piezoelectric sensing material.

4.6 References

[1] Sarıyer, D.; Küçer, R.; Küçer, N. Neutron Shielding Properties of Concretes Containing Boron Carbide and Ferro–Boron. Procedia-Social and Behavioral Sciences, 2015, 195, 1752-1756.

[2] Murty, K. Linga. Introduction to Nuclear Materials: Fundamentals and Applications. 2013.

[3] D. A. Parks and B. R. Tittmann, "Radiation Tolerance of Piezoelectric Bulk Single-Crystal Aluminum Nitride," IEEE Transactions on Ultrasonics, Ferroelectrics, and Frequency Control, Vol. 61, No. 7, pp. 1216-1222, 2014.

[4] Was, Gary S. Fundamentals of Radiation Materials Science: Metals and Alloys. Springer-Verlag New York, 2018.

[5] Kerrigan, Sean P. High Temperature Embedded/Integrated Sensors (HiTEIS) for Remote Monitoring of Reactor and Fuel Cycle System. 2019, pp. 4–7, High Temperature Embedded/Integrated Sensors (HiTEIS) for Remote Monitoring of Reactor and Fuel Cycle System

[6] Kim, Howuk, et al. "Accelerometer with AlN Bulk Single Crystals for Nuclear Power Plants." Sensors, 2020.

CHAPTER 5

EFFECT OF TEMPERATURE ON SENSOR MATERIALS AND THE WIRELESS COMMUNICATION NETWORK'S RESPONSE

5.1 Background

The next generation of nuclear power plants include reactors designs that operate at much higher temperatures compared to currently operating commercial reactors. The Very-High-Temperature Reactor (VHTR) is one of the Gen. IV designs that can reach operating temperatures upwards of 1000 °C. While designing instrumentation and sensors to outfit the next generation of reactors, the sensors must be tested to ensure they can withstand the harsh operating environments of the next generation nuclear power plants.

Fiber optics are commonly used for high-temperature applications due to the their high operating temperature and high resistivity to electromagnetic interference [1]. Fiber optics offer significant advantages due to their small size and lightweight design. Fiber optics are immune to electrical interference, thus they are able to be inserted into a large number of systems. Fiber optics provide measurements of several different system parameters such as strain, temperature, liquid level, and vibration while offering a sensing medium that is corrosion resistant and are typically nonflammable [2]. Piezoelectric and fiber optic-based vibration sensors are used throughout the NPP industry due to their durability at high temperatures. Fiber optics are more expensive than piezoelectric sensors and undergo a complicated fabrication process [3]. The performance of the piezoelectric material depends on the environmental conditions of the sensor. Piezoelectric sensors have a simple structure, are cost effective, and high frequency resolution making them favorable for NPP applications if they can survive the harsh environment [4].

Despite the advantages of piezoelectrics over fiber optics, piezoelectrics are Piezoelectric sensors are favored over fiber optics due to their cheaper fabrication cost and simpler design; however, the lifetime of the sensor can significantly impact the cost/benefit analysis of this sensor design [5]. If a piezoelectric sensor can be fabricated that can operate reliably and efficiently at high-temperatures, then this would bridge the gap between the advantage fiber optics have over piezoelectrics under these conditions.

5.2 Objectives

In order to ensure the sensor can withstand the operating environment of the VHTR, high-temperature sensor performance testing is conducted. This research aims to study the effect of temperature on sensor performance and wireless communication networks that would be utilized during measurements on the VHTR. The effects of temperature must be studied as they effect the physical elements of the sensor due to prolonged high-temperature exposure and the electrical performance of the sensor. By designing a test to monitor and measure the sensor performance as temperature increases, the sensor's applicability to the VHTR design can be determined.

5.3 Materials & Methods

In order to characterize the influence of temperature of the sensor and wireless communication network, two different tests were performed using high temperature furnaces. Each test aimed to study either the effect of temperature on the sensor or wireless communication network [6].

5.3.1 Sensor Performance within a High-Temperature Environment and Prolonged Exposure Testing

The fabricated vibration sensor was characterized on its performance throughout a high-temperature environment of 600 °C to 1000 °C. The system setup is shown in Fig. 5.1. The input of a vibration signal is determined by the Function Generator. A harmonic signal from the Function generator is fed into a Power Amplifier. The amplified signal is fed into the vibration shaker which simulates the vibration effects. The vibration sensor is mounted to the top of a connecting rod which is connected to the vibration shaker. The actuation of the vibration shaker causes the connecting rod to move which generates a set vibration signal for the vibration sensor to process. The high-temperature accelerometer is located within a high-temperature furnace to control the temperature within ± 1 °C. The output signal of the vibration sensor is relayed through two platinum wires that are connected to a Charge Amplifier. The charge amplifier converts the charge signal to a voltage signal which is finally displayed and recorded on the oscilloscope.

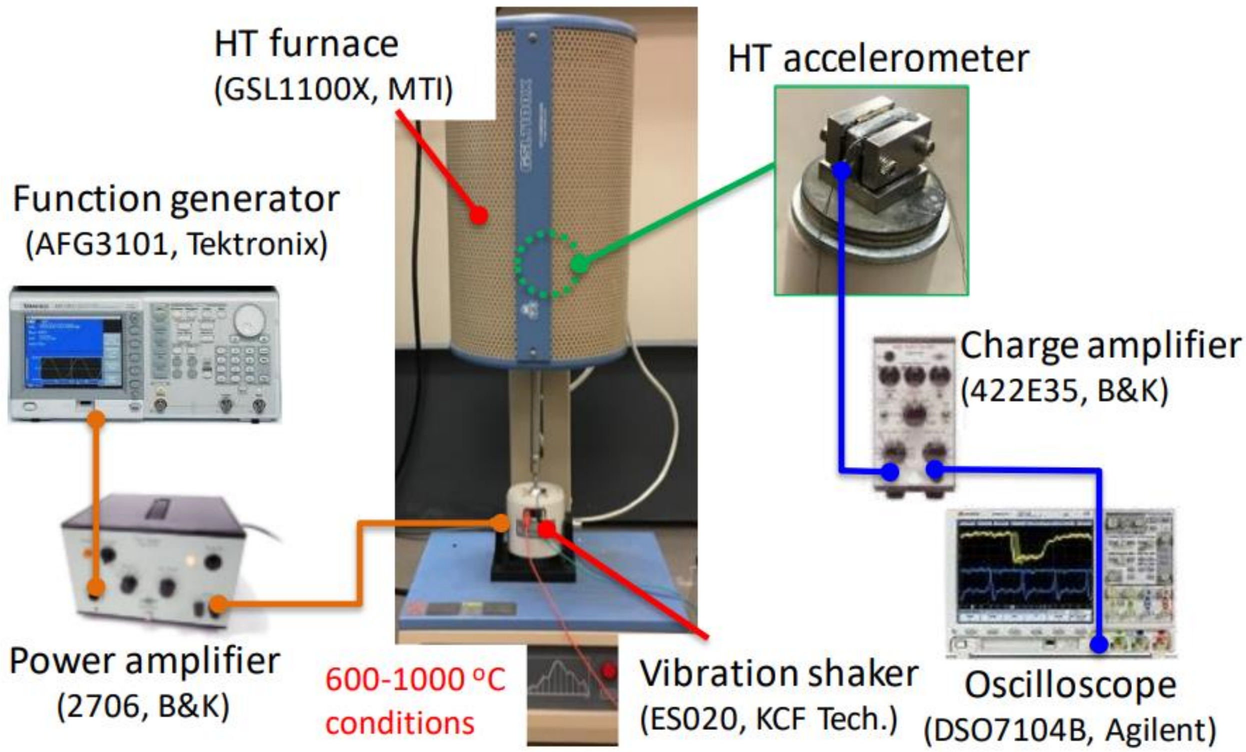

Figure 5.1. Setup for high-temperature testing of the AlN-based vibration sensor.

5.3.2 Performance Evaluation of the Wireless Communication Network while Sensor Exposed to High-Temperatures

The wireless communication network transmits the output data from the sensor to a wireless display that a nuclear power plant operator views. The quality of the information output by the signal is influenced by the performance of the sensor itself and the functionality and efficiency of the communication network. In order to understand the performance of the wireless communication network, a similar system setup to the one reference prior was used. The vibration sensor was mounted to the top of a rod connecting the sensor to the vibration shaker as shown in Fig. 5.2. The input to the vibration shaker was set using the pulse generator and power amplifier. The difference between the previous run tests involves the output of the sensor. The output of the sensor was connected to a charge amplifier in order to convert the output charge signal to a voltage signal. The signal is passed through a noise filter to both eliminate noise and amplify the output signal to millivolts range. The processed signal is fed into an Analog-to-Digital Convertor (ADC), which allows for quick sampling rate to be obtained. The ADC must sample the data twice as fast as the signal changes to ensure no loss of information when recreating the signal for digital display. The processed data is fed from the ADC to a Raspberry Pi that transmits the data wirelessly to a digital display. The performance of the sensor was measured at temperatures ranging from room temperature to 1000°C.

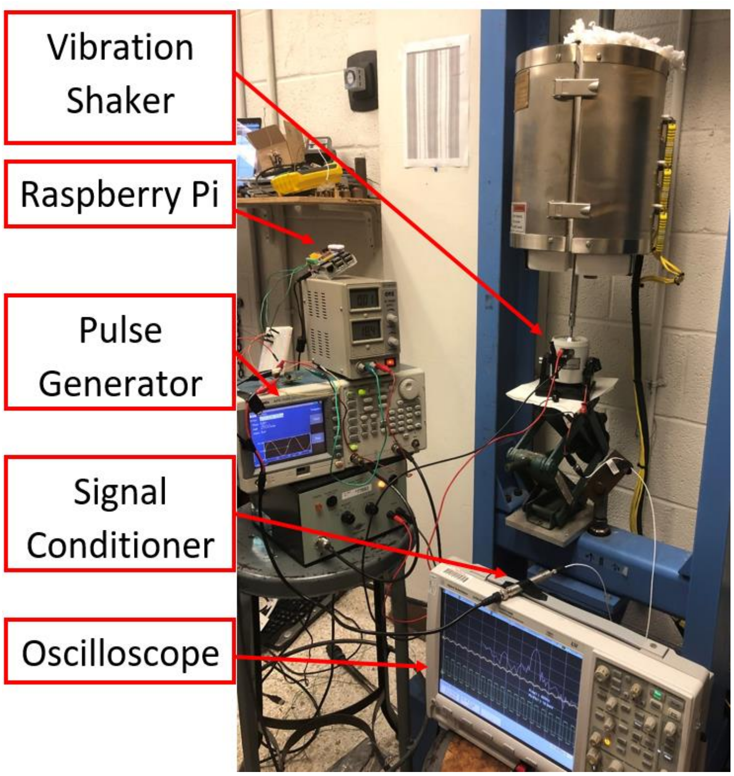

Figure 5.2. Setup for high-temperature testing of the AlN-based vibration sensor and the wireless communication network.

Data was acquired by manipulating the system parameters including frequency, vibration amplitude, and the furnace temperature. The system parameters were changed using the following bounds:

Frequency: {40 Hz, 100Hz, 200 Hz}

Vibration amplitude: {14mV, 28mV, 42mV, 56mV, 70mV, 84mV, 250mV, 500mV, 750mV, 1000mV, 1250mV, 1500mV}

Furnace temperature: {200 °C, 400 °C, and 600 °C}

5.4 Results & Discussion

5.4.1 Vibration Sensor Characterization within a High-Temperature Environment

The high-temperature analysis of the vibration sensor showed constant sensor response up to temperatures of 1000 °C as shown in Fig. 5.3. The sensor response did not vary much with changes in frequency or temperature, thus the sensor response performs successfully across a wide temperature and frequency range.

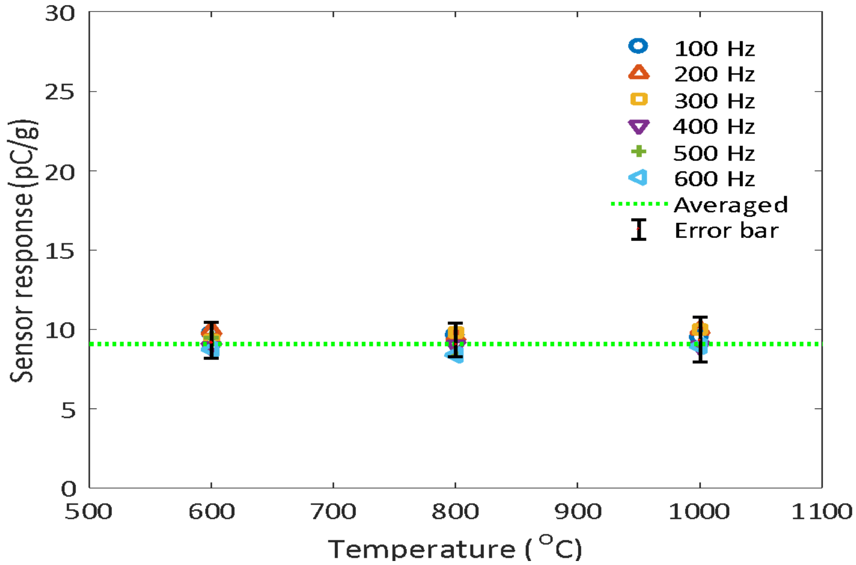

Figure 5.3. Sensor response as a function of temperature.

An endurance test was performed using the exact system setup shown in Fig. 5.1. The performance of the sensor at 1000 °C for a period of 10 hours was recorded. The results, shown in Fig. 5.4 (a), proved the sensor response showed little to no variation in performance or functionality for a prolonged period of time within a high-temperature environment. The high-temperature accelerometer was able to successfully capture vibrational response data with no impact on the output signal as a function of temperature. The high-temperature testing did impact the lifetime of the sensor as the effect of the high-temperature environment can be seen in Fig. 5.4 (b) after a period of 10 hours exposure to 1000 °C. Despite the consistent high performance of the vibration sensor within the high-temperature region, the prolonged exposure of the sensor impacted the expected lifetime of the sensor as the structural materials may begin to separate or fail. The intended application for the sensors involves placing the sensors outside of the reactor core. The sensor would be placed outside the RPV and transmit data wirelessly, thus the sensor is non-intrusive and the sensor does not require specific placement. The sensing technology allows for the sensor to be adequately shielded from the harshest environment in a nuclear power plant. Thus, the sensor should never experience temperatures upwards of 1000 °C; however, the tests prove that the sensor is capable of performing under this high-temperature condition. For these reasons, the effect of temperature on the wireless communication system must also be studied as the sensor output is only successful if the information is transmitted to a wireless display for power plant operators to view without interruption or signal decay.

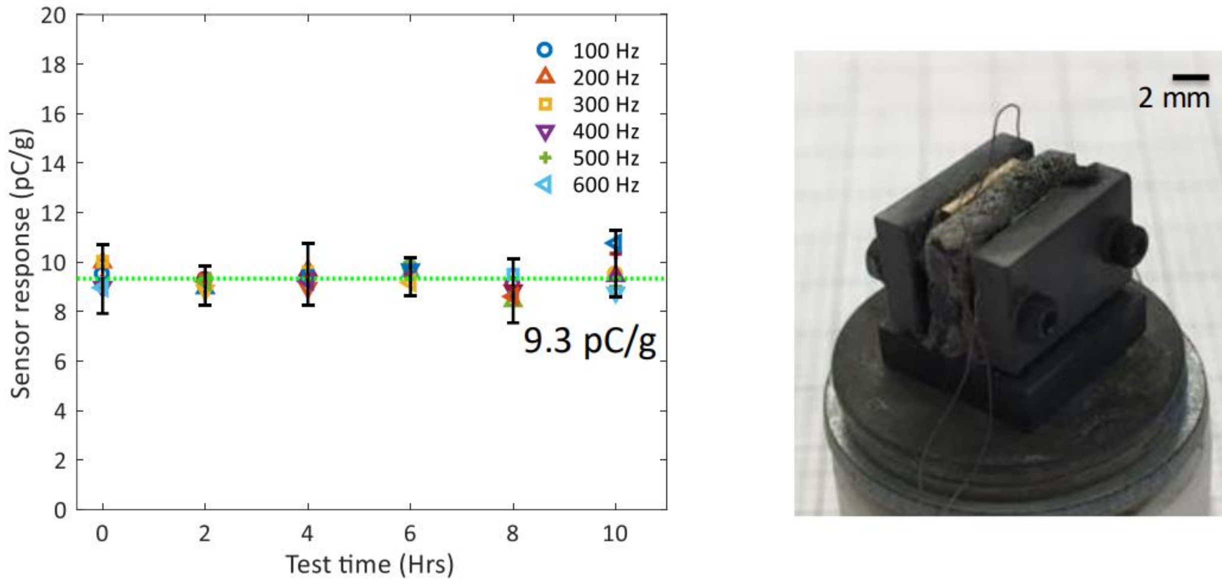

(a) (b)

Figure 5.4. Sensor response output over an extended period of time at high temperature (a), and a photo of the vibration sensor after the prolonged high temperature test (b).

5.4.2 Performance of the Wireless Communication System while Sensor Operates within a High-Temperature Environment

The results of these tests are shown in Fig. 5.5 at 100 Hz. The frequency displayed by the wireless communication system showed the same frequency experienced by the vibration sensor. The transmitted data shows slight alterations likely caused by either energy loss during transmission through the communication network or changes caused during the filtering process. When an increase in vibration amplitude occurs, it can be seen that an increase in the peak power of the transmitted signal occurs; however, this shift does not depend on temperature. Fig. 5.6 shows that throughout the tested temperature range, the vibration sensor maintains a linear behavior, thus the sensor and wireless communication network performance is not impact by high-temperature environments.

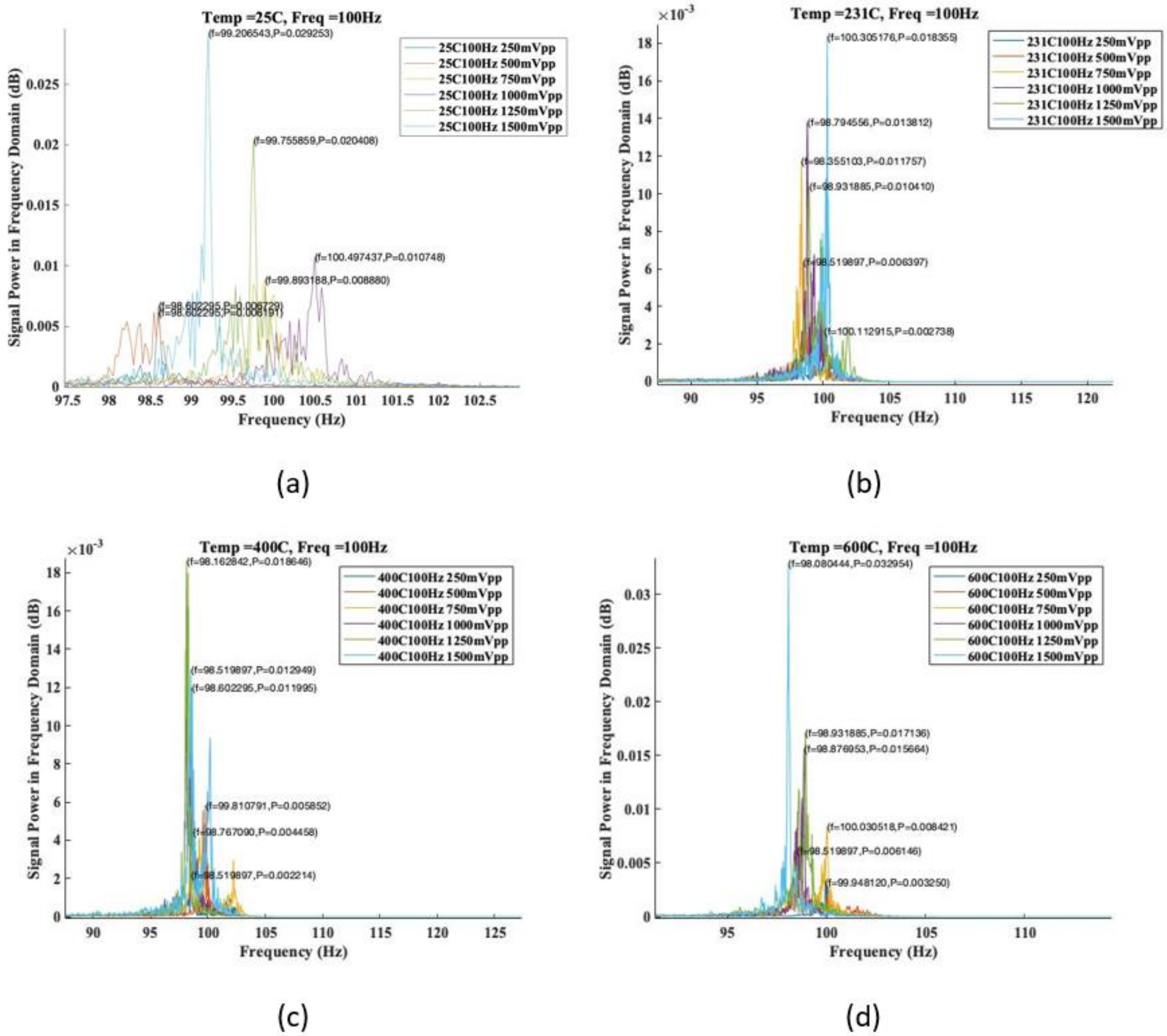

Figure 5.5. The frequency response of the measured and wirelessly communicated data from the vibration sensor at different temperatures and vibration amplitude and frequency of 100 Hz.

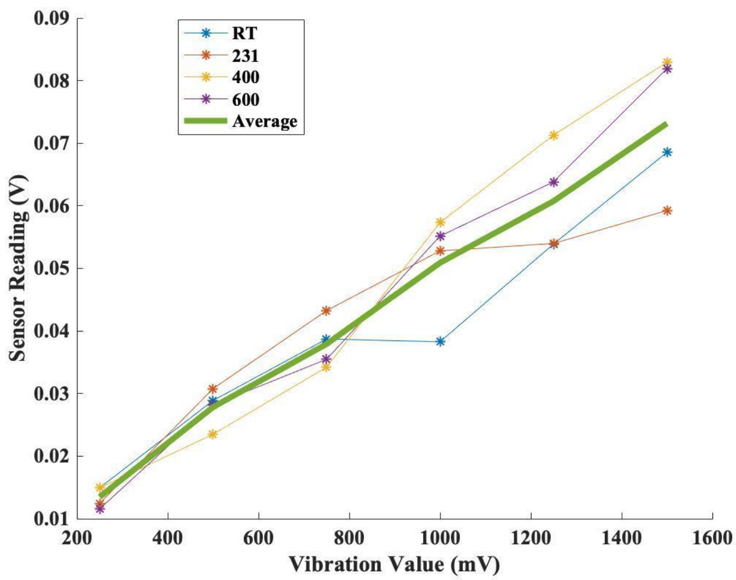

Figure 5.6. The vibration voltage magnitude and corresponding processed sensor reading at 100 Hz.

The same procedure was carried out using higher (200 Hz) and lower (40 Hz) frequencies to see if the sensor or wireless communication networks performance were affected. The amplitude of vibration was also reduced to determine the sensitivity of the wireless communication network. The results, shown in Fig. 5.7, show that at low frequencies and low vibration amplitudes, the wireless communication network is able to successfully acquire, process, and transmit the data to a digital display, making the system ideal for nuclear power plant applications. At a low frequency of 40 Hz, the sensor once again maintains a linear relationship between the input vibration level and the sensor output as shown in Fig. 5.8.

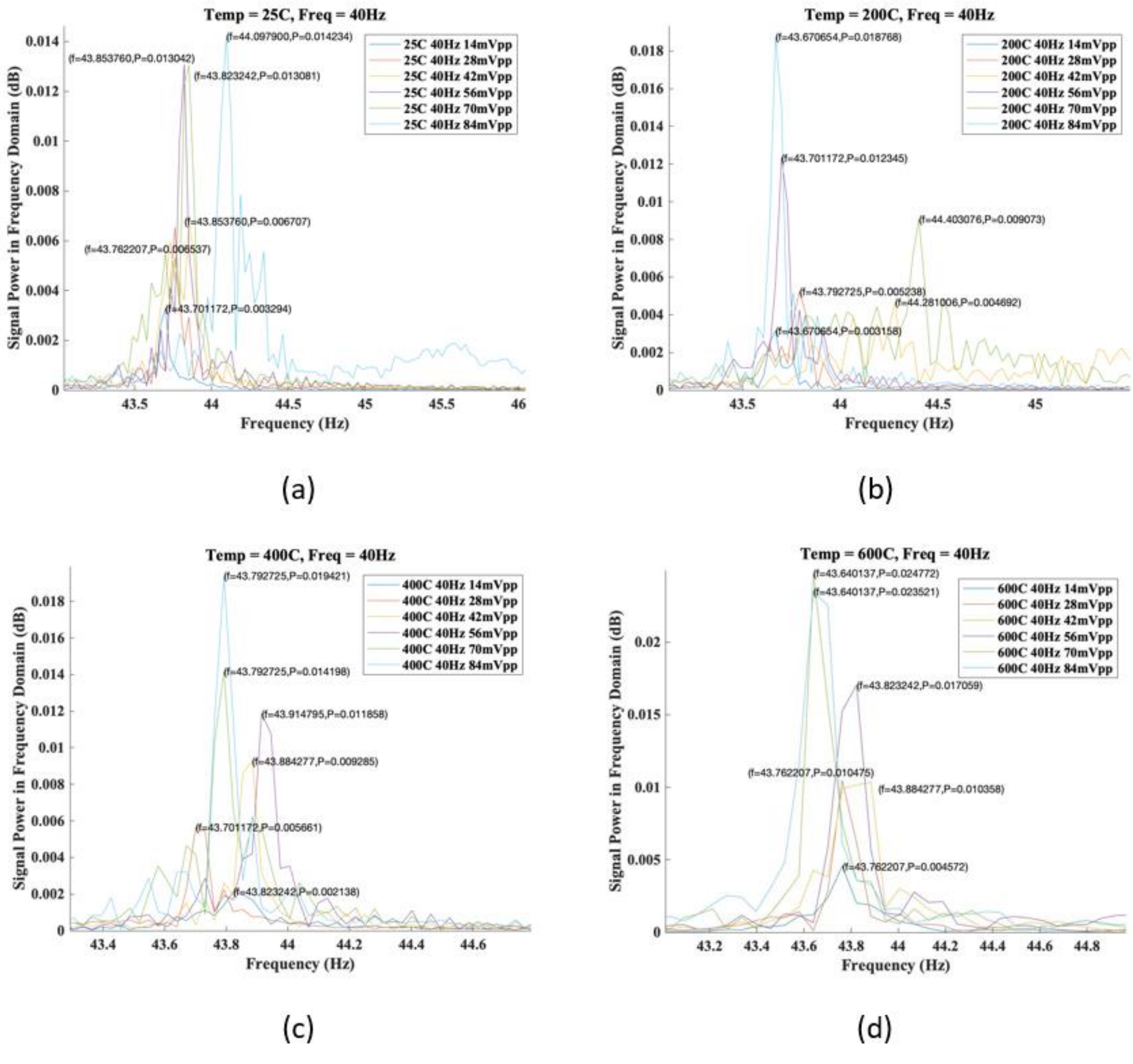

Figure 5.7. The frequency response of the measured and wirelessly communicated data from the vibration sensor at different temperatures and vibration amplitude and frequency of 40 Hz.

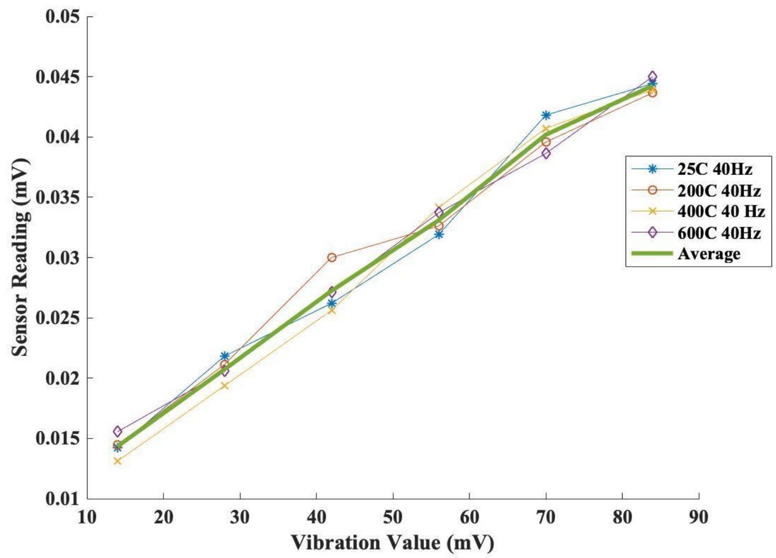

Figure 5.8. The vibration voltage magnitude and corresponding processed sensor reading at 40 Hz.

5.5 Conclusions

The VHTR can reach operating temperatures of 1000 °C, but it is unlikely the proposed sensor or communication network would ever experience temperatures of that range due to the system being wireless and non-intrusive. The results of the high-temperature testing showed that the performance of the AlN vibration sensor was not impacted by temperature changes up to 1000 °C. The manufactured vibration sensor showed noticeable charring of the sensor elements, which may impact the lifetime of the device, but the output data showed no variation with increasing temperature. Upon testing the wireless communication network, a series of tests were performed by changing the frequency, vibration amplitude, and furnace temperature to measure the sensor and communication networks performance under a combination of frequencies and vibration amplitudes while the sensor operated at high-temperatures. The study found that the wireless communication network was able to successfully acquire, process, and transmit data to a digital display across a sensor operating temperature range up to 600 °C. The developed AlN vibration sensor and communication network are able to function reliably and efficiently up to temperatures of 1000 °C, making it an ideal sensor for next generation nuclear power plants.

5.6 References

[1] Kasinathan, M., Sosamma, S., BabuRao, C., Murali, N.; Jayakumar, T. (2012). Fiber optic sensors for Nuclear Power Plant Applications. AIP Conference Proceedings. https://doi.org/10.1063/1.4716333

[2] Krohn, D. A., MacDougall, T.; Mendez, A. (2014). Fiber optic sensors: Fundamentals and Applications. SPIE Press. Gupta, B. D. Fiber Optic Sensors: Principles and Applications, New India Publishing, 2006.

[3] Partridge, A.; Reynolds, J. K.; Chui, B. W.; Chow, E. M.; Fitzgerald, A. M.; Zhang, L.; Kenny, T. W. A High-Performance Planar Piezoresistive Accelerometer. Journal of Microelectromechanical Systems, 2000, 9, 58-66.

[4] Hashemian, H. M. (2006). Maintenance of process instrumentation in nuclear power plants. Springer.

[5] Hashemian, H. M. (1987). Degradation of nuclear plant temperature sensors. Division of Engineering, Office of Nuclear Regulatory Research, U.S. Nuclear Regulatory Commission.

[6] B. Balagopal, S. Kerrigan, H. Kim, M. Chow, M. Bourham and X. Jiang, “A Smart Sensor Prototype for Vibration Sensing in Nuclear Power Plants,” 2019 IEEE 28th International Symposium on Industrial Electronics (ISIE), Vancouver, BC, Canada, 2019, pp. 1127-1132.

CHAPTER 6

EFFECT OF ZrO_2 THIN-FILM COATINGS AND IRRADIATION ON THE CORROSION RATE OF SENSOR MATERIALS

6.1 Background

Nuclear power plants utilize over 10,000 sensors and detectors to monitor plant performance [1]. Instrumentation and Controls (I&C) relay information to power plant operators who use the information to control system performance. Nuclear power plants operate using several different types of sensors to control and monitor temperature, flow, pressure, and neutron flux [2]. Nuclear power plant I&C ensure the system operates safely and reliably.

The proposed next generation of reactors, Gen. IV, utilizes reactors that operate at much higher temperatures than currently operational commercial power plants. The VHTR can reach operating temperatures of 1000 °C [3]. Current I&C approaches need to be modified in order to accommodate the high operating temperate of the VHTR design. Invasive sensors are not designed to withstand the environmental conditions of the VHTR. By researching applications of non-intrusive sensing, wireless sensors provide similar sensing functionality to invasive sensors without needing to withstand the harsh environmental conditions.

Sensors outfitted to nuclear power plants must ensure reliable and stable operation within harsh environmental conditions, consisting of high-temperature (HT), radiation damage, or corrosion [3,4]. Piezoelectric sensors using aluminum nitride (AlN) as the active sensing element offer promising performance in harsh environmental conditions. AlN exhibits a curie temperature of 1200 °C and maintains high thermal conductivity, low thermal expansion, and high electrical resistivity, making it an ideal material for use within harsh environmental conditions especially at high-temperatures [5]. H. Kim et al. developed a high-temperature AlN accelerometer with stable performance at high-temperature (1000 °C) and gamma irradiation (~12 kGy) conditions [6]. The sensor has been shown to withstand the environmental effects of high-temperature and radiation. Corrosion effects can also cause material failure, thus this paper investigates the performance of AlN single crystals for use in piezoelectric accelerometers. The effects of temperature, pH, thin-film coatings, and irradiation on the corrosion rate are presented and discussed.

Accelerated corrosion tests are performed by running cyclic polarization corrosion experiments using a Gamry© corrosion cell to analyze the long-term corrosion effects over short time scales. During cyclic polarization testing, an external voltage or current is applied while the other is measured in response [7]. The application of an external voltage perturbs the equilibrium state, thus achieving a state of polarization. Cyclic polarization testing allows for the effects of corrosion to be observed over short time scales despite the mechanism of corrosion being a relatively slow process [8]. By performing corrosion experiments, the corrosion rate of a material can be measured, thus the expected lifetime of a material can be calculated.

Within an electrochemical reaction consisting of anodic and cathodic reactions, the Butler-Volmer equation (Eq. 6.1) shows the relationship between the potential and current:

$$I = I_{corr}(exp\left[\frac{\alpha_a nF(E - E_{corr})}{RT}\right] - exp\left[\frac{-\alpha_c nF(E - E_{corr})}{RT}\right]) \tag{6.1}$$

Where:

I is the measured current (A),

Icorr is the corrosion current (A),

αa and αb are the anodic and cathodic charge transfer coefficients,

n is the number of electrons within the reaction,

F is Faraday's constant (= 9.6485E+04 C/mol),

Ecorr is the corrosion potential (V),

R is the universal gas constant (= 8.3145 J/(mol-K)),

T is the absolute temperature (K).

The term 2.3RT/αnF is typically written as ß, therefore Eq. 6.1 becomes [9]:

$$I = I_a + I_c = I_{corr}(\exp\left(\frac{2.3\eta}{\beta_a}\right) - \exp(\frac{2.3\eta}{\beta_c})) \tag{6.2}$$

Where:

Ia and Ic are the anodic and cathodic currents (A),

η is the overpotential (η = E – Ecorr, (V)),

ßa and ßc are the anodic and cathodic Tafel slopes (V/decade).

When isolating the potential to a region of low overpotential (i.e. close to the corrosion or equilibrium potential), the exponential terms may be expanded using a Taylor Series about η = 0 [10]. The resulting equation is the Stern-Geary equation:

$$\left.\frac{d\eta}{dI}\right|_{\eta\to 0} = \frac{\beta_a\beta_c}{2.3I_{corr}(\beta_a + \beta_c)} \tag{6.3}$$

The slope of the potential versus current curve near the equilibrium potential is referred to as the polarization resistance, Rp. Solving Eq. 6.3 for the corrosion current gives the following equation:

$$I_{corr} = \frac{\beta_a\beta_c}{2.3R_p(\beta_a + \beta_c)} \tag{6.4}$$

All terms in Eq. 6.4 can be determined experimentally, thus the corrosion current can be calculated. The following equation can be used to determine the corrosion rate of a given material to the corrosion current:

$$CR = \frac{I_{corr}\ k\ EW}{\rho\ A_c} \tag{6.5}$$

Where:

CR is the corrosion rate of a given material in mm per year (mmpy),

k is a constant (= 3272 mm/(A-cm-yr)),

EW is the equivalent weight of the electrode (g),

ρ is the mass density of the sample (g/cm3),

Ac is the exposed area of the sample to the corrosive solution (cm2).

Cyclic polarization corrosion experiments calculate the corrosion rate of a material using Eq. 6.5. The lifetime of the material as a function of failure due to corrosion can be estimated once the corrosion rate is known. Thin-film coatings are commonly used throughout the electronics industry to protect, improve, and enhance the performance and lifetime of microelectronics. The high operating temperature of the VHTR creates a corrosive environment that can lead to material failure if not shielded. Zirconium alloys have been used as cladding with nuclear power plants due to their high corrosion resistance [11]. With a melting temperature of 2680 °C and high corrosion resistivity, zirconium dioxide (ZrO_2) thin-films can mitigate the effects of corrosion and extend the lifetime of a material [12].

6.2 Objectives

The Very-High Temperature Reactor (VHTR) is a proposed generation IV reactor design that can reach operating temperatures of 1000 °C. The next generation of nuclear power plants offer a material challenge to current reactor sensing technologies. Gen. IV reactor designs operate under harsh environmental conditions, thus current commercial sensors will not survive within these environments. Development of wireless, non-intrusive AlN based piezoelectric vibration sensors aim to provide the VHTR with reliable and safe sensing. The effects of corrosion on the sensor can impact the performance and expected operational lifetime of the sensor.

This research aims to analyze the effect of corrosion on AlN single crystals that will be used to create accelerometer devices for use in the Gen. IV reactor designs. The effect of thin-film coatings of ZrO_2 will be investigated to determine how they impact the corrosion rate of the material especially at higher temperatures. The effect of temperature, pH level, and irradiation on the corrosion rate will be analyzed. By understanding the mechanism of corrosion on the samples, an estimated sensor lifetime can be calculated, which will help determine the maintenance schedule of a nuclear power plant due to sensor failure.

6.3 Materials & Methods

Single crystal samples of AlN with geometric dimensions of 8 mm x 1.25 mm x 1.3 mm were fabricated by HexaTech, Inc. (Morrisville, NC). The single crystals were grown in the [0 0 0 1] c-axis to obtain thickness-shear mode samples. Thin-film coatings of ZrO_2 were deposited on the AlN single crystal samples using Atomic Layer Deposition (ALD) at the Analytical Instrumentation Facility (AIF) on North Carolina State University's campus. ALD offers thin-film deposition with minimal impact to the surface of the AlN single crystal. Other deposition techniques were considered, such as Physical Vapor Deposition (PVD) and Chemical Vapor Deposition (CVD). The physical bombardment of atoms onto the surface of the electrode coating disrupts the electrical performance of the sensor, thus PVD was not selected as the deposition technique [13]. CVD operates using a volatile precursor that reacts with the sample surface, thus both vapor deposition techniques were not selected [14]. ALD provides thin-film coatings with a very low deposition rate with minimal impact to the substrate surface [15].

Sample irradiation was performed using a Cobalt-60 irradiator (Gammacell 220, MDS Nordion, Ottawa, Canada) within North Carolina State University's Nuclear Engineering Department. Samples of AlN single crystals were placed within a plastic container inside the Co-60 irradiator for periods of 1 and 2 months. The additive total dose accumulated by the samples was estimated to be 11.2 kGy and 19.2 kGy for the 1 month and 2 month samples, respectively.

Electrochemical cyclic polarization corrosion experiments were performed within a 3-electrode Gamry cell: the working electrode consisting of the AlN single crystal, the counter electrode consisting of a graphite rod, and the reference electrode consisting of a Ag/AgCl solution. The electrochemical corrosion cell was filled with prepared solutions of pH values of 3 and 6 using potassium nitrate (KNO_3) and drops of sulfuric acid (H_2SO_4). The corrosion cell was placed within a heated water bath to regulate the temperature up to 80 °C. The setup of the electrochemical corrosion cell is shown in Fig. 6.1. The corrosion rate was estimated using the Gamry Instruments (Warminster, PA) MULTIPORT™ Interface 1000 potentiostat connected to the electrode cell.

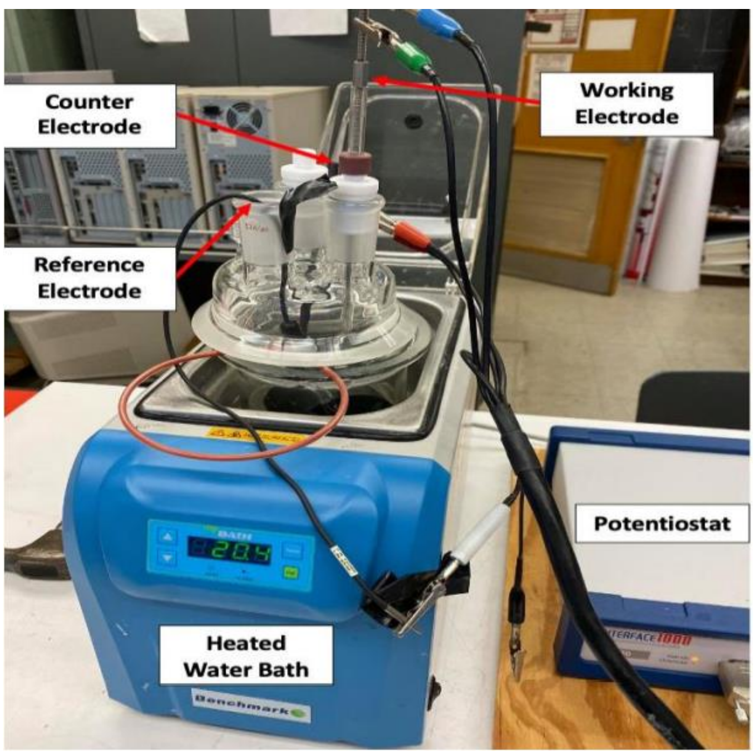

Figure 6.1. Electrochemical corrosion cell setup to cyclic polarization corrosion tests.

Table 6.1. Measured material properties of AlN single crystals for corrosion rate calculations.

Mass (g)	0.0434
Density (g/cm^3)	3.266
Exposed Area (cm^2)	0.0494
Equivalent Weight (g)	13.663

Data analysis of the corrosion curves was performed using Gamry Instruments Echem Analyst™ Software. The anodic and cathodic Tafel constants were measured by calculating the slope of the anodic and cathodic curves within the software as shown in Fig. 6.2. The polarization resistance, R_p, was measured by applying linear regression to the low potential region within ±5 mV of E_{corr}. Throughout cyclic polarization testing, the forward voltage scan is swept ± 250 mV with a scan rate of 0.6 mV/s. The material properties used to calculate the corrosion rate of the sample using Eq. 6.5 are shown in Table 6.1. Typically, cyclic polarization corrosion experiments are performed using conductive metals having large exposed areas. This research offers insight into performing corrosion experiments on small exposed areas using semi-conducive materials.

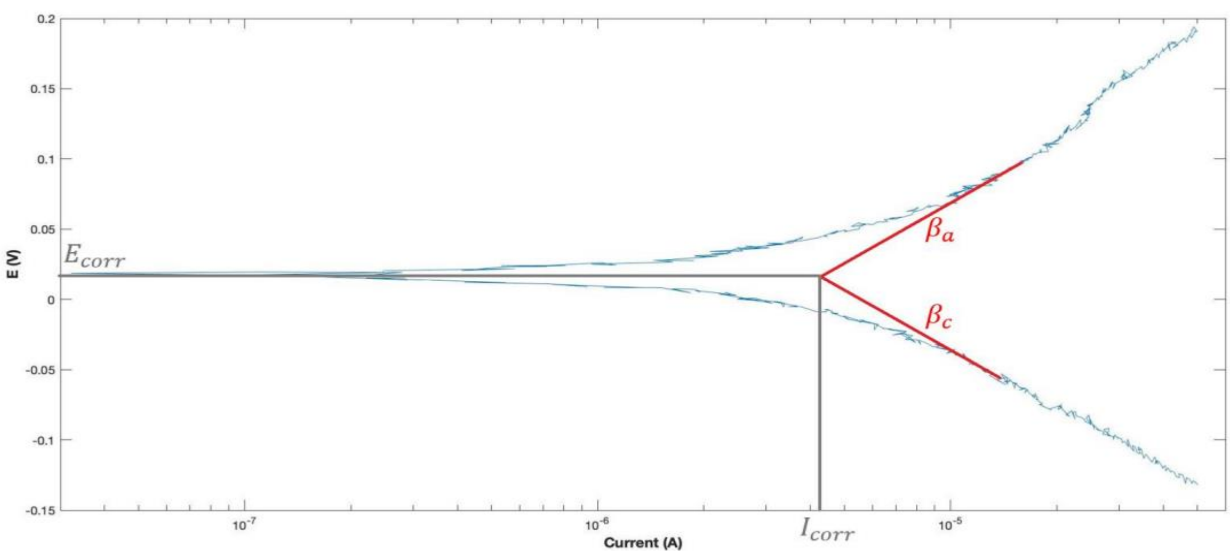

Figure 6.2. Cyclic polarization corrosion curve showing the anodic and cathodic curves.

6.4 Results & Discussion

Samples of bare and 100 nm thick ZrO_2 coated samples were observed using pH values of 3 and 6 up to a temperature of 80 °C. The corrosion test displays signs of instability at temperatures higher than 80 °C, thus data extrapolation of the corrosion curve was employed. Data extrapolation was used by modeling a power-law fit to predict the corrosion rate up to 200 °C as shown in Equation 6.6. The power-law model was selected as the extrapolation method due to the strong fit at higher temperatures. An exponential extrapolation method was also considered that fit better at low temperatures (< 100 °C), but the results were not logical at high temperatures. For these reasons, the power-law model was used to extrapolate all corrosion rate data up to 200 °C. The predicated corrosion rates through extrapolation seem reasonable.

$$CR = A * T^B \tag{6.6}$$

Where:

CR is the corrosion rate in (mmpy)

T is the temperature in Celsius (°C)

A and B are constants dependent on the function

The corrosion rate of bare and ZrO_2 coated samples is shown in Fig. 6.3. The corrosion rate increased with increasing temperature and increasing acidity (lower pH). The coated samples showed a lower corrosion rate compared to the bare samples regardless of the observed solution pH value, which indicates an effective protective coating. The lifetime of the sensor is shown in Fig. 6.4 where the bare samples exhibit an expected lifetime of between 5-10 years at room temperature which further decreases as temperature increases. When comparing the lifetime of the bare AlN crystals to the coated samples, the coating extends the lifetime of the sensor by over 1.5 times at room temperature. The coated samples were shown to have an expected lifetime of 9.1 years and 12.9 years at pH values of 3 and 6, respectively. Analyzing the effect of the lifetime extension due to the addition of a thin-film ZrO_2 coating as a function of temperature is shown in Fig. 6.5. At room temperature, the 100 nm thick coating of ZrO_2 provides a lifetime extension of 4-5 years that decreases with increasing temperature. At 200 °C, the coatings provide between 0.5-1.5 years lifetime extension, which is a 78% increase over the bare sample at a pH of 6 and a 38% increase over the bare sample at a pH of 3. The 100 nm thick thin-films of ZrO_2 were able to provide improved corrosion resistance that extended the lifetime of the samples across the temperature range when compared to the bare samples. By increasing the thickness of the thin-film coating or utilizing additional coatings to form multi-layered coatings, the lifetime of the sensor could be increased further [16]. Another method for controlling the lifetime of the sensor involves regulating the temperature the sensor is exposed to by using insulation or constructing a sensor housing to further shield the single crystal from the improved corrosion rate observed at higher temperatures.

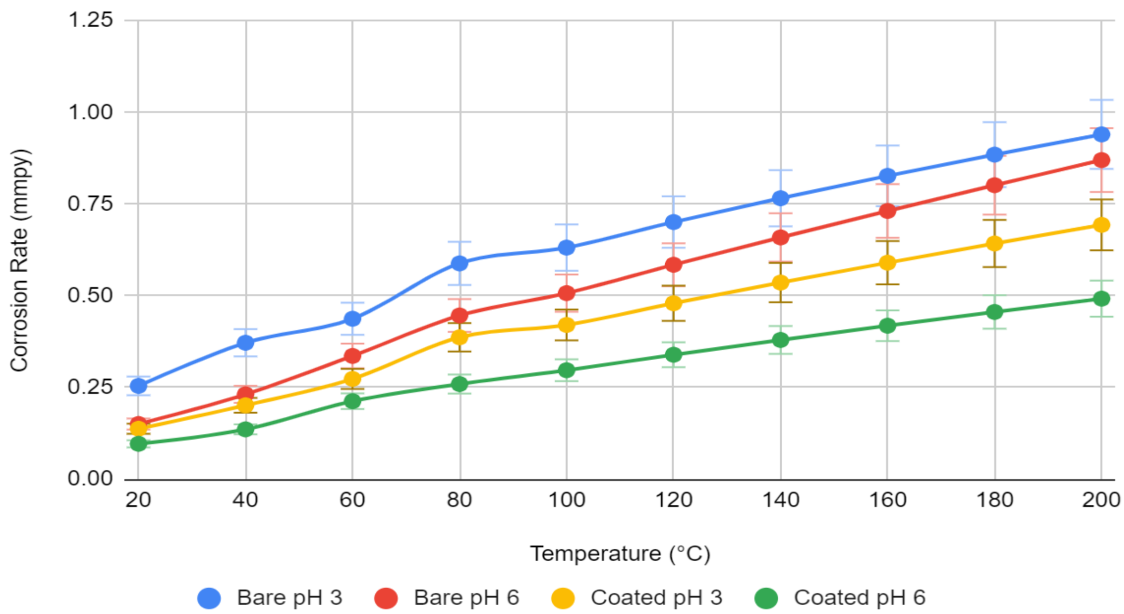

Figure 6.3. Corrosion rates of bare and ZrO_2 coated samples of AlN single crystal sensing elements at pH values of 3 and 6.

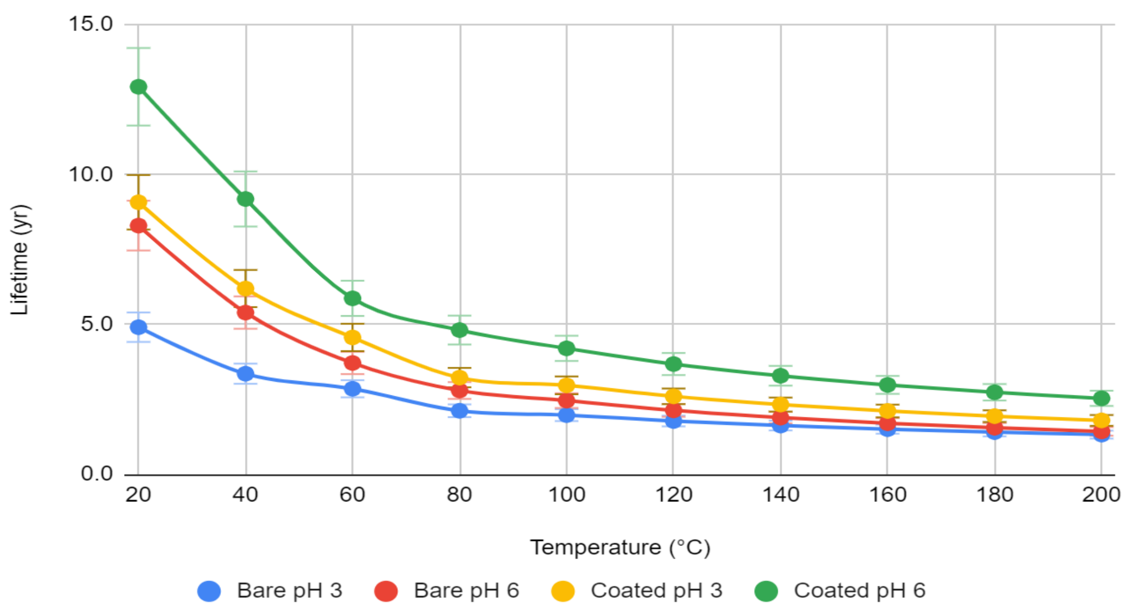

Figure 6.4. Lifetime of bare and ZrO_2 coated AlN single crystal sensing elements at pH values of 3 and 6.

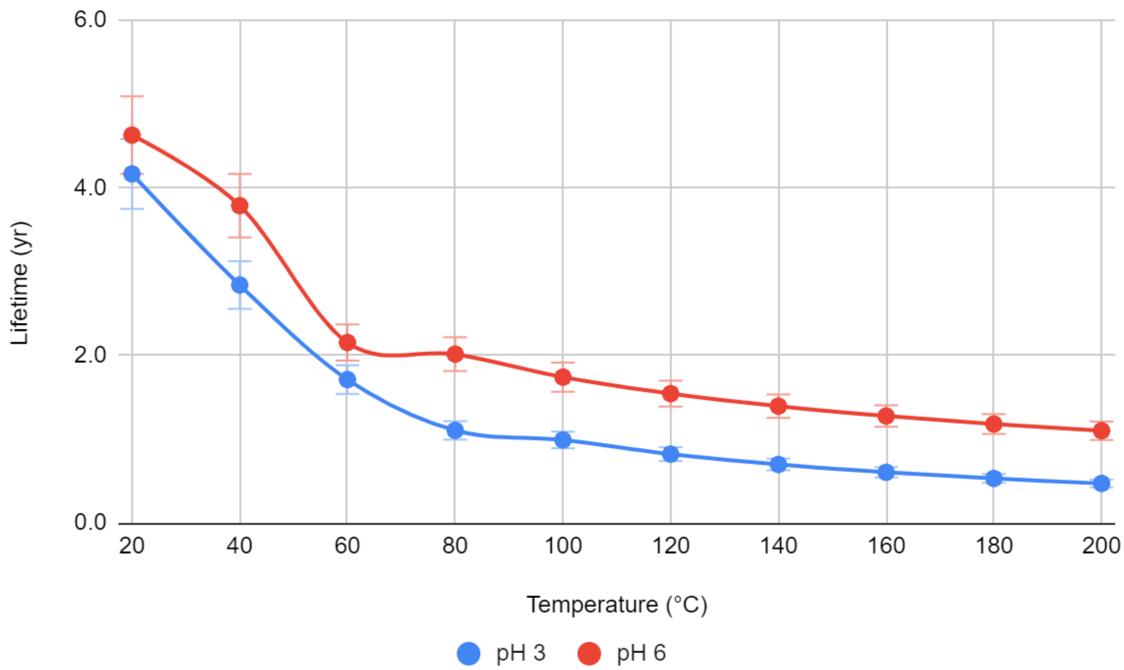

Figure 6.5. Lifetime enhancement of the thin-layer ZrO_2 coating at pH values of 3 and 6.

The effect of irradiation on the corrosion rate of AlN single crystals is shown in Fig. 6.6. Samples of AlN were exposed to a Co-60 gamma source for a period of 1 or 2 months that accumulated a total dose of 11.2 kGy and 19.3 kGy, respectively. The corrosion rate was observed to increase with increasing temperature. As temperature increased, the samples that were irradiated exhibited a sharper rise of the corrosion rate when compared to non-irradiated samples. At 200 °C, the corrosion rate of the irradiated samples was 4.5 times as large as the bare sample and 6.1 times as large as the coated sample with a pH of 3. Lifetime analysis of the irradiated samples compared to the bare and coated samples at a pH of 3 is shown in Fig. 6.7. At room temperature, a difference can be observed between the 1 month and 2 month irradiated samples; however, the corrosion behavior of these samples grow closer at higher temperatures leading to a similar estimated lifetime. When comparing the lifetime of the irradiated samples to the bare and coated samples of

AlN, the irradiation of the AlN sensing element decreases the corrosion resistance of the material, thus increasing the observed corrosion rate and decreasing the estimated lifetime of the sensor after irradiation. The sensor should be shielded by irradiation to inhibit the effects of irradiation through either additional thin-film coatings or a fabricated sensor housing to shield the sensor during operation.

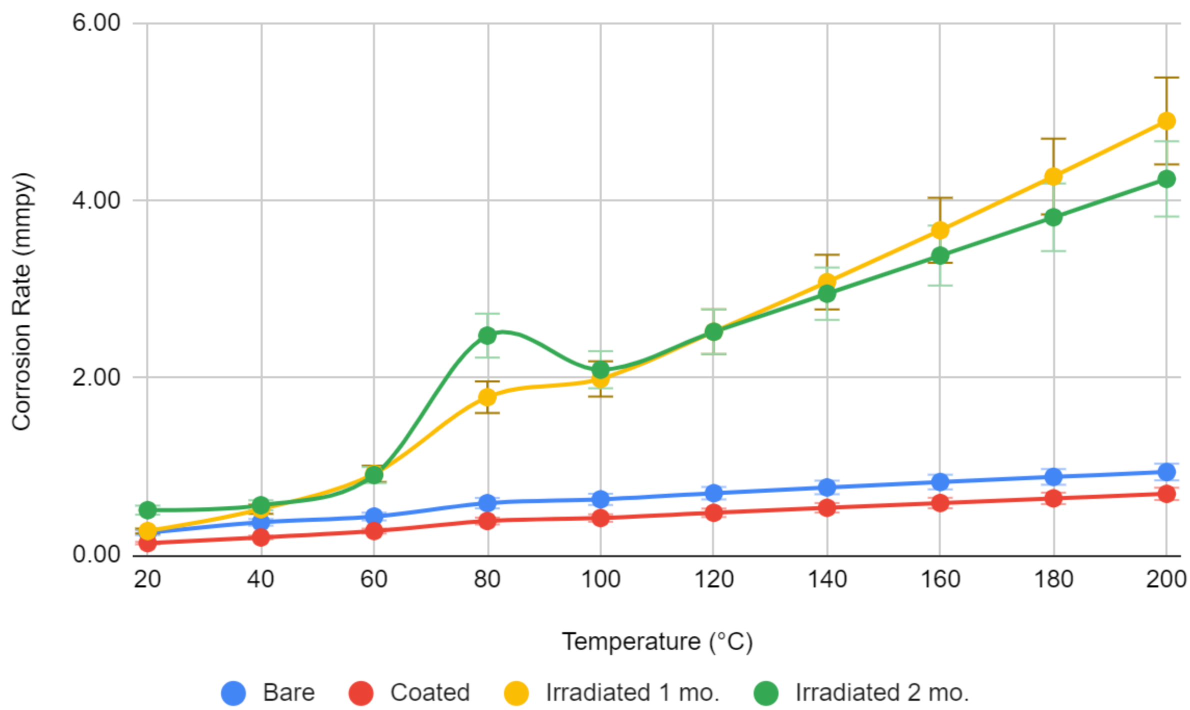

Figure 6.6. Corrosion rates of bare, ZrO_2 coated, and irradiated samples of AlN single crystal sensing elements at a pH value of 3 for 1 month and 2 months.

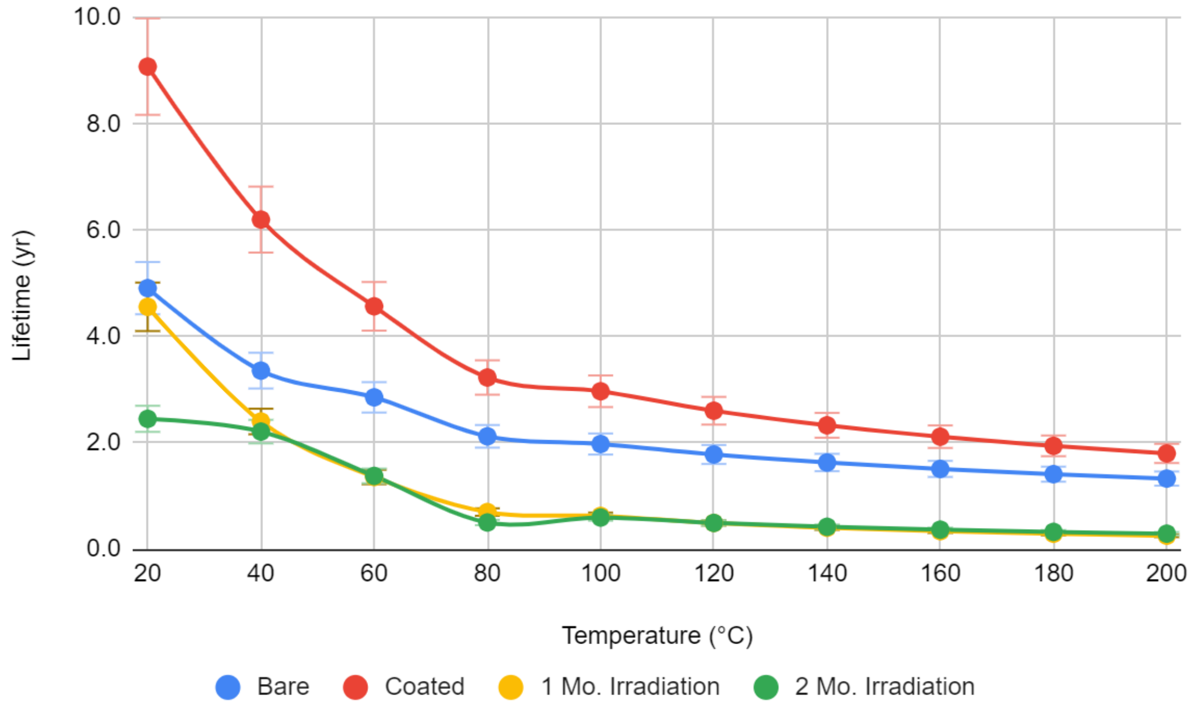

Figure 6.7. Lifetime of bare, ZrO_2 coated, and irradiated samples of AlN single crystal sensing elements at a pH value of 3 for 1 month and 2 months.

The effect of thin-film coatings of ZrO_2 and irradiation on the corrosion behavior of AlN single crystals was observed by performing cyclic polarization corrosion tests. Samples deposited with thin-film coatings of ZrO_2 showed reduced corrosion rates when compared to bare AlN single crystal samples. The addition of thin-film ZrO_2 coatings extended the sensor lifetime by 4 to 5 years at room temperature and 0.5 to 1.5 years at 200 °C depending on the pH. The effect of irradiation on the AlN single crystals was investigated by irradiating samples using a Co-60 gamma source for periods of 1 and 2 months. The corrosion rate analysis showed a much higher corrosion rate than the bare or coated samples at a pH of 3. As such, the estimated lifetime of the sensor after irradiation decreased when compared to the non-irradiated samples. There are several ways to improve the lifetime of the sensor by reducing the measured corrosion rate. One method involves utilizing thicker coatings of ZrO_2 to enhance the effect the coating provides especially at higher temperatures. Additional thin-films coatings of other materials could also be added to provide shielding against effects shown to increase the corrosion rate such as pH, temperature, and irradiation.

6.5 Conclusions

Piezoelectric accelerometers are used in nuclear power plants to detect structural damage that can cause the plant to shut down for maintenance. In order to extend the operational lifecycles of commercial next-generation nuclear power plants, wireless non-intrusive piezoelectric vibration sensors using AlN as the active sensing element were fabricated. The corrosion analysis of bare AlN single crystals showed a corrosion rate that increased with temperature and increased as the acidity (lower pH) increased. The addition of thin-film coatings was explored by utilizing ALD to coat 100 nm layers of ZrO_2 onto the surface of the AlN single crystals. The cyclic polarization corrosion tests on coated samples revealed similar trends to the bare samples; however, the comparison between coated and bare samples revealed that the coating was able to extend the lifetime of the sensors by ~5 years at room temperature and ~1 year at 200 °C at a pH of 6. Single crystal AlN samples were irradiated using a Co-60 gamma source for periods of 1 and 2 months that achieved cumulative doses of 11.2 kGy and 19.3 kGy, respectively. At a pH of 3, the comparison between the irradiated samples and a bare sample showed a noticeable increase in the corrosion rate of the irradiated samples. At room temperature, the bare sample showed an estimated lifetime prediction of ~5 years while the sample irradiated for 2 months exhibited a lifetime prediction of only ~2.5 years. As temperature increased, the 1 and 2 month irradiated samples revealed similar lifetime prediction models while the bare (non-irradiated) sample showed a significantly higher lifetime expectation. The corrosion analysis of AlN single crystals showed viability for use in the next generation of nuclear power plants as the lifetime of the sensors provided a lifetime estimation that fits within nuclear power plants operating schedules. The lifetime of the sensors was shown to increase by 1 to 5 years depending on temperature and pH as 100 nm thin-films were added. If additional coatings or thicker coatings are added to the sensor, the lifetime could be further expanded or provide protection from the effects of irradiation.

6.6 References

[1] Korsah, K. (2009). Instrumentation and controls in nuclear power plants: An emerging technologies update. U.S. Nuclear Regulatory Commission, Office of Nuclear Regulatory Research.

[2] IAEA. (1984). *Nuclear power plant instrumentation and control: A guidebook*.

[3] Ingersoll, D. T. (2005). Status of physics and safety analyses for the liquid-salt-cooled very high-temperature reactor (LS-VHTR). https://doi.org/10.2172/885991

[4] Cattant, F., Crusset, D., & Féron, D. (2008). Corrosion issues in nuclear industry today. *Materials Today, 11(10), 32-37*. doi:10.1016/s1369-7021(08)70205-0

[5] Jiang, X., Kim, K., Zhang, S., Johnson, J., & Salazar, G. (2013). High-temperature piezoelectric sensing. *Sensors, 14(1), 144–169*. https://doi.org/10.3390/s140100144

[6] Kim, H., Kerrigan, S., Bourham, M., Jiang, X. (2021). ALN Single Crystal Accelerometer for Nuclear Power Plants. *IEEE Transactions on Industrial Electronics, 68(6), 5346–5354*. https://doi.org/10.1109/tie.2020.2992002

[7] Stansbury, E. E., Buchanan, R. A. (2004). *Fundamentals of Electrochemical Corrosion*. ASM International.

[8] Murty, K. L., Charit, I. (2013). *An introduction to nuclear materials fundamentals and applications*. Wiley-VCH-Verl.

[9] Petrii, O. A., Nazmutdinov, R. R., Bronshtein, M. D., Tsirlina, G. A. (2007). Life of the Tafel equation: Current understanding and prospects for the second century. *Electrochimica Acta, 52(11), 3493–3504*. https://doi.org/10.1016/j.electacta.2006.10.014

[10] Stern, M. (1957). Electrochemical polarization. *Journal of The Electrochemical Society, 104(11), 645*. https://doi.org/10.1149/1.2428438

[11] Than, Y. R., Wenman, M. R., Grimes, R. W. (2020). Cu and SB in Tetragonal ZrO2 on fuel cladding. *Journal of Applied Physics, 128(13)*, 135101. https://doi.org/10.1063/5.0021174

[12] Botzakaki, M. A., Xanthopoulos, N., Makarona, E., Tsamis, C., Kennou, S., Ladas, S., Georga, S. N., Krontiras, C. A. (2013). ALD deposited ZrO2 ultrathin layers on Si and Ge substrates: A multiple technique characterization. Microelectronic Engineering, 112, 208–212. https://doi.org/10.1016/j.mee.2013.03.002

[13] Lee, B., et al. “A Novel Thermally-Stable Zirconium Amidinate ALD Precursor for ZRO2 Thin Films.” *Microelectronic Engineering*, vol. 86, no. 3, 2009, pp. 272–276., doi:10.1016/j.mee.2008.03.020.

[14] Sivaram, S. *Chemical Vapor Deposition: Thermal and Plasma Deposition of Electronic Materials*. Springer, 1995.

[15] Hwang, Cheol Seong. *Atomic Layer Deposition for Semiconductors*. Springer, 2014.

[16] Fusco, Michael A., et al. “Corrosion of Single Layer Thin Film Protective Coatings on Steel Substrates for High Level Waste Containers.” *Progress in Nuclear Energy*, vol. 89, 2016, pp. 159–169., doi:10.1016/j.pnucene.2016.02.016.

CHAPTER 7

SUMMARY, CONCLUSIONS, AND FUTURE WORK

7.1 Summary

The next generation of nuclear power plants requires advanced instrumentation and controls to monitor power plant performance. Vibration sensors are essential to ensure the structural stability of key reactor components. Sensors must be designed using more resilient materials to ensure the sensors can operate in harsher environments similar to those prevalent in the next generation of nuclear power plants. A vibration sensor was designed, fabricated, and tested in Chapter 2 using bulk seismic mass and active sensing element that provides a higher sensitivity over previously studied sensing materials. The initial sensor design operates uni-axially, thus a multi-axial vibration sensor was designed and fabricated to determine if the location of the source vibration could be identified rather than simply intensity. This work researched how to test the applicability of the fabricated sensor using a Mock-Up experiment aimed to simulate a few measurable parameters present within a nuclear reactor in Chapter 3. This proved to be a viable method as testing an experimental sensor on an operation nuclear power plant was not an option and the majority of Gen. IV nuclear power plants are still in the design phase. The remainder of this research aimed at testing the viability of the AlN active sensing material within a harsh environment.

The VHTR operates at high-temperatures that can damage materials placed inside them. The VHTR is a nuclear reactor, thus sensor materials must be robust against radiation effects. Finally, the high-temperature produced by this reactor design generates a highly corrosive environment that can degrade the structural integrity of the sensor and cause it to fail. Investigation into the effects of high-temperature, radiation, and corrosion on the sensor and AlN active sensing material were researched. The effects of radiation, temperature, and corrosion on the sensor and AlN active sensing element are investigated in Chapter 4, Chapter 5, and Chapter 6 respectively.

7.2 Conclusions

Several conclusions are reached from the results of this research:

- A piezoelectric accelerometer using AlN single crystals as the active sensing material was designed and fabricated for use in harsh environments generated by the proposed next generation of nuclear power plants. A multi-axial accelerometer was designed, simulated, and fabricated to determine if the location of a input vibration signal can be determined. The simulations from the multi-axial vibration sensor show each axis having a working frequency range from 0 to 350 Hz. The fabricated very was able to sense weak amplitudes of incoming vibrations, though further amplification would be needed to refine the sensor performance.
- In order to simulate the sensor performance within the target application for these sensors, a reactor mock-up system was designed to mimic several measurable parameters within a nuclear power plant. These parameters included: temperature,

liquid level, flow rate, and vibration. The fabricated AlN-based accelerometer was outfitted to the outside of the mock-up steel tank. Output data was recorded from the sensor while altering the flow rate of the incoming streams to determine if the sensor could notice a change in signal when this occurs. The preliminary sensor data showed the feasibility of the sensor to operate within a nuclear power plant application.

- The effect of irradiation was determined by exposing AlN single crystal samples and a fully fabricated accelerometer to a Co-60 gamma source for 1 and 2 months. SEM and EDS analysis was performed pre and post irradiation, showing no viable changes in surface topography or composition as a result of gamma exposure.
- The effect of neutron exposure was simulated using a 14 MeV monoenergetic hydrogen beam. The results showed that the incident angle of the beam affected the penetration depth of the particles. The beam parallel to the surface of the Inconel 601 housing demonstrated the lowest surface penetration depth but showed a wide array of target damage across the surface. The beam perpendicular to the surface of the Inconel 601 housing showed the greatest penetration depth, but the damage was confined to the width of the beam. The Inconel 601 housing material provided sufficient shielding for the AlN active sensing material to not be impacted by incoming gamma-rays or neutrons.
- High-temperature testing showed that the performance of the AlN vibration sensor was not impacted by temperature changes up to 1000 °C. Prolonged high-temperature exposure tests showed noticeable charring on the sensor housing, but the output data showed no variation at elevated temperatures. The developed AlN

vibration sensor was able to successfully acquire data with exposed to temperatures up to 1000 °C, and the wireless communications system was able to transmit the data reliably and efficiently.

- The corrosion analysis of bare AlN single crystals showed that the corrosion rate increased with temperature and increased as the pH of the solution decreased.
- AlN single crystals were irradiated using a Co-60 gamma source for a period of 1 and 2 months to achieve cumulative doses of 11.2 kGy and 19.3 kGy. The comparison between irradiated and non-irradiated samples showed the irradiated samples exhibiting a higher corrosion rate. The estimated lifetime of the sensing element at room temperature was ~5 years while the 2 month irradiated sample was only ~2.5 years.
- The addition of (~100 nm) thin-film coatings of ZrO2 on the surface of the AlN single crystals proved to enhance the lifetime of the sensor as the temperature increased. The addition of thin-film ZrO2 coatings extended the sensor lifetime by 4 to 5 years at room temperature and 0.5 to 1.5 years at 200 °C depending on the pH.
- Based on the research of this project, the materials characterization of AlN under exposure to high-temperatures, irradiation, and corrosive effects showed that AlN is a robust and reliable material for use in the next generation of nuclear power plants as the active sensing material for fabricated piezoelectric accelerometers.

7.3 Future Work

7.3.1 Corrosion Studies

The corrosion studies demonstrated the value of adding thin-film coatings to the sensor material to better shield them from corrosive effects, especially as temperature increased. To further identify the impact that thin-film coatings can have on the sensor, different coatings should be tested to observe how the performance of other thin-film coatings compares to the ZrO2 tested. The major limiting factor of the coating in the project was the thickness. As only 100 nm thin-films were used, investigation into how the thin-film thickness affects both the corrosion rate and the sensor performance should be investigated. This will help shield the sensor during VHTR operations.

The corrosion data was measured to 100 °C and then extrapolated up to 200 °C as this is the intended operating temperature of the sensor while being placed outside of the reactor pressure vessel. As the intended goal is to identify if the sensor materials can survive the operating temperatures of the VHTR design, an autoclave should be used to run corrosion experiments upwards of the 1000 °C target of the VHTR. The other parameter during corrosion studies that showed a impact on the corrosion rate was the pH of the solution used. As only two different solutions were used at a pH of 3 and 6, there should be another study to observe the effects of a basic solution on the sensor.

7.3.2 Multi-Axial Sensor Performance and Calibration

The simulation results from the multi-axial sensor showed promise towards being able to detect the same signal from three different axis simultaneously. The goal of the research aims to use the sensor output to be able to identify the source of the vibration signal. If the sensor maintains a high sensitivity, identifying the location of the source signal could be important so proper maintenance can be done in the correct area. The sensing element performance analysis showed consistent measurements with previously fabricated sensors. The problem shifted when fabricating the multi-axial sensor with the seismic mass. When connected to the vibration shaker, the sensor was able to measure signals however, the intensity of these signals was competing with high baseline noise. Further research would need to be done to analyze techniques to enhance the intensity of the output sensor signals and then measure the sensor output signals at different angles using the device shown in Fig 7.1. The output signals for each of the three axis would be compared to determine if the incident angle of vibration can be determined.

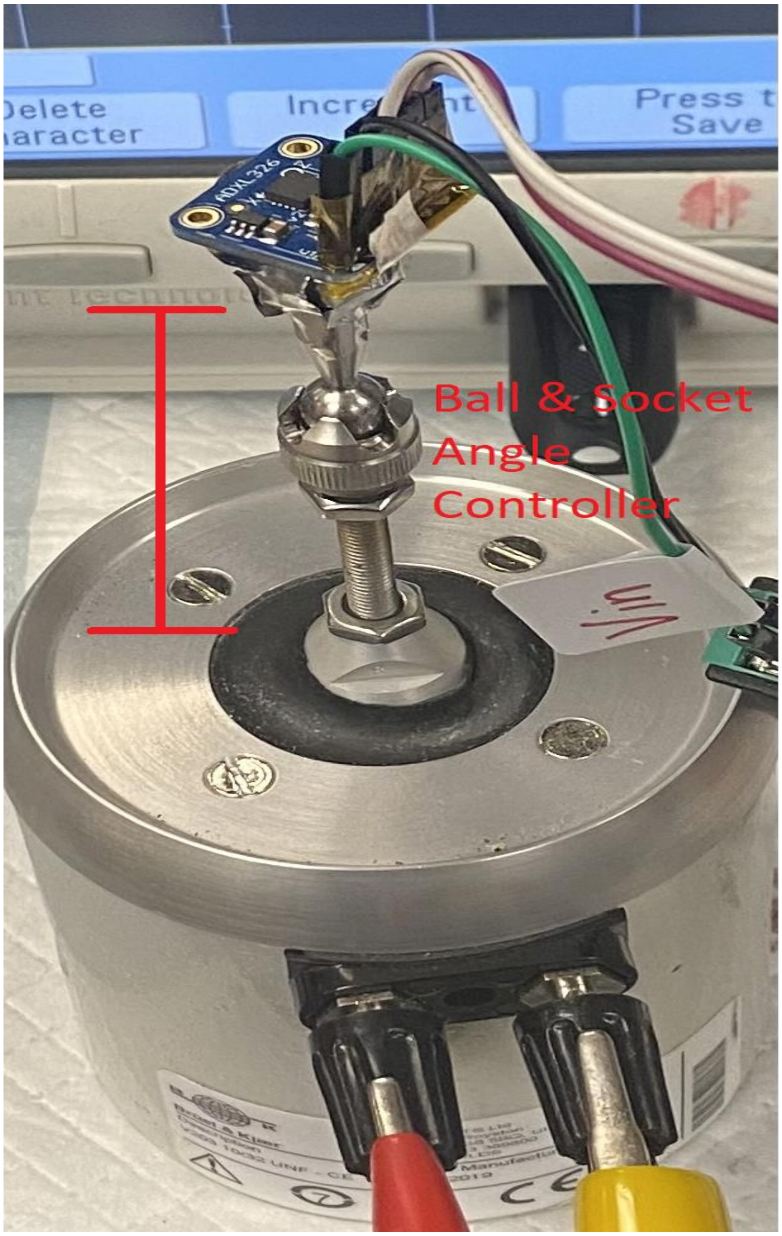

Figure 7.1. Vibration shaker with fabricated ball & socket angle controller attached (pictured at a 0° angle).

APPENDIX

Appendix A - MatLab Code to Process Sensor Output

```
clear all

filepath = '';%file path
filename = '';%file name
filename1 = [filepath filename];
myfile = csvread(filename1,2,0,[2,0,1001,2]);
myTime = myfile(:,1);
myAmp = myfile(:,3);
% myfile2 = csvread(filename1,1004,0,[1004,0,2003,1]);
% myFreq = myfile2(:,1);
% myMag = myfile2(:,2); %frequency domain if any
figure
set (gca,'position',[0.15,0.15,0.69,0.69] )

line(myTime*1e6,myAmp,'linewidth',3)
% xlim([4.3 5.5]) %Time domain
% ylim([-1 1])    %Amplitude

ax1 = gca ;
ax1_pos = ax1.Position;
% ax1.XColor = 'g';
% ax1.YColor = 'g';

xlabel('Times(\mus)');
ylabel('Amplitude(V)')
set(ax1,'Fontsize',14)
set(ax1,'linewidth',1.5)
%% Enable frequency domain if any
% ax2 = axes('Position',ax1_pos,...
%     'XAxisLocation','top',...
%     'YAxisLocation','right',...
%     'Color','none');
%
% line((myFreq/1e6),myMag,'Parent',ax2,'linewidth',3)
% xlim([20 40])
% % ylim([-15 0.2])
% xlabel('Frequency(MHz)')
% ylabel('dB')
% set(ax2,'Fontsize',14)
% set(ax2,'linewidth',1.5)
Vpp = (max(myAmp)-min(myAmp)) % Maximum value
```